

Multidecadal North Atlantic sea surface temperature and Atlantic meridional overturning circulation variability in CMIP5 historical simulations

Liping Zhang^{1,2} and Chunzai Wang²

Received 22 May 2013; revised 4 September 2013; accepted 8 September 2013; published 23 October 2013.

[1] In this paper, simulated variability of the Atlantic Multidecadal Oscillation (AMO) and the Atlantic Meridional Overturning Circulation (AMOC) and their relationship has been investigated. For the first time, climate models of the Coupled Model Intercomparison Project phase 5 (CMIP5) provided to the Intergovernmental Panel on Climate Change Fifth Assessment Report (IPCC-AR5) in historical simulations have been used for this purpose. The models show the most energetic variability on the multidecadal timescale band both with respect to the AMO and AMOC, but with a large model spread in both amplitude and frequency. The relationship between the AMO and AMOC in most of the models resembles the delayed advective oscillation proposed for the AMOC on multidecadal timescales. A speed up (slow down) of the AMOC is in favor of generating a warm (cold) phase of the AMO by the anomalous northward (southward) heat transport in the upper ocean, which reversely leads to a weakening (strengthening) of the AMOC through changes in the meridional density gradient after a delayed time of ocean adjustment. This suggests that on multidecadal timescales the AMO and AMOC are related and interact with each other.

Citation: Zhang, L., and C. Wang (2013), Multidecadal North Atlantic sea surface temperature and Atlantic meridional overturning circulation variability in CMIP5 historical simulations, *J. Geophys. Res. Oceans*, 118, 5772–5791, doi:10.1002/jgrc.20390.

1. Introduction

[2] The oceans play a crucial role in the climate system. Ocean currents move substantial amounts of heat, most prominently from the lower latitudes where heat is absorbed by the upper ocean, to higher latitudes where heat is released to the atmosphere. This poleward transport of heat is a fundamental driver of the climate system and has crucial impacts on the distribution of climate. One of the most prominent ocean circulation systems is the Atlantic Meridional Overturning Circulation (AMOC). As described by previous studies [e.g., Bryden *et al.*, 2005; Wunsch and Heimbach, 2006; Zhang, 2008, 2010], this circulation system is characterized by northward flowing warm and saline water in the upper layer of the Atlantic Ocean, cooling and freshening of the water at higher northern latitudes of the Atlantic in the Nordic and Labrador Seas, and southward flowing colder water at depth. This circulation transports heat from the South Atlantic and tropical North Atlantic to the subpolar and polar North Atlantic, where heat is

released to the atmosphere with substantial impacts on climate over large regions.

[3] The AMOC has a large multidecadal variability. However, there is no consensus for the physical mechanisms of the AMOC fluctuations. Some studies argue that the AMOC variability is an ocean-only mode excited by or damped by atmospheric forcing [Frankcombe *et al.*, 2009]. Other studies claim that the AMOC is primarily an ocean mode with density fluctuations in the convection regions driven by advection of density anomalies from the low latitudes [e.g., Vellinga and Wu, 2004] or the northern high latitudes such as the Arctic Ocean [e.g., Delworth *et al.*, 1993; Jackson and Vellinga, 2012]. The AMOC is also deemed as a fully coupled atmosphere-ocean or atmosphere-sea ice-ocean mode with the deep water formation rate dominated by variations in the local wind forcing [e.g., Dickson *et al.*, 1996; Häkkinen, 1999; Eden and Willembrand, 2001; Deshayes and Frankignoul, 2008; Msadek and Frankignoul, 2009; Medhaug *et al.*, 2012]. Regardless of the detailed mechanisms mentioned above, the low-frequency variability of the AMOC is usually accompanied with the anomalous northward heat transport in the upper ocean, which in turn can affect the Atlantic SST. This is one of the most common associations used to explain the Atlantic Multidecadal Oscillation (AMO) [Folland *et al.*, 1984; Gray *et al.*, 1997; Delworth and Mann, 2000; Knight *et al.*, 2005; Wang and Zhang, 2013; Zhang *et al.*, 2012]. Additionally, the multidecadal period of the AMO may originate from the AMOC, since the deep ocean has a longer memory compared to the atmosphere and the upper layer ocean.

¹Cooperative Institute for Marine and Atmospheric Studies, University of Miami, Miami, Florida, USA.

²NOAA/Atlantic Oceanographic and Meteorological Laboratory, Miami, Florida, USA.

Corresponding author: L. Zhang, NOAA/Atlantic Oceanographic and Meteorological Laboratory, 4301 Rickenbacker Causeway, Miami, FL 33149, USA. (Liping.Zhang@noaa.gov)

[4] The AMO can be defined in different ways, though the resulting time series are similar. *Parker et al.* [2007] defined the AMO as the third rotated empirical orthogonal function (EOF) of low frequency worldwide observed SST, while *Mestas-Nuñez and Enfield* [1999] defined the AMO as the first rotated EOF of the non-ENSO global SST. The AMO index can also be defined as the detrended area-weighted SST from the Atlantic western coast to the eastern coast and from 0°N to 60°N [e.g., *Knight et al.*, 2005; *Sutton and Hodson*, 2005]. Many regional climate phenomena and weather events have been found to link with the AMO, such as the Northeast Brazilian and African Sahel rainfall [*Folland et al.*, 1986; *Rowell et al.*, 1995; *Folland et al.*, 2001; *Rowell*, 2003; *Wang et al.*, 2012], Atlantic hurricanes [*Goldenberg et al.*, 2001; *Wang and Lee*, 2009], North American and European summer climate [*Enfield et al.*, 2001; *McCabe et al.*, 2004; *Sutton and Hodson*, 2005; *Knight et al.*, 2006; *Folland et al.*, 2009; *Sutton and Dong*, 2012; *Wang et al.*, 2013; *Zhang and Wang* 2012], and summer SST variability in coastal China sea [*Zhang et al.*, 2010]. Although the most popular explanation is that the AMO is induced by the internal variability of the AMOC [*Kravtsov and Spannagle*, 2008; *Knight*, 2009; *Ting et al.*, 2009], the mechanism of the AMO is still unclear. Some model simulations indicate that solar variability, volcanoes, and/or anthropogenic aerosol variability contribute to setting the AMO phase [*Hansen et al.*, 2005; *Otterå et al.*, 2010] or even predominantly determine [*Booth et al.*, 2012] the AMO variability. A recent observational study shows that a positive feedback between the SST and dust aerosol in the North Atlantic via Sahel rainfall variability may be a mechanism for the AMO [*Wang et al.*, 2012]. However, to what extent the aerosol can contribute to the AMO is still unclear. *Zhang et al.* [2013] rebut the argument of *Booth et al.* [2012] since there are major discrepancies between the HadGEM2-ES simulations and observations in the North Atlantic Ocean.

[5] *Medhaug and Furevik* [2011] examine the connection between the AMO and AMOC using a full range of the Coupled Model Intercomparison Project phase 3 (CMIP3) or the Intergovernmental Panel on Climate Change (IPCC) Fourth Assessment Report (AR4) climate simulations for the 20th century. They find that, in most climate models, the increased SST in the North Atlantic is associated with a stronger than normal AMOC. Recently, IPCC has initiated the Fifth Assessment Report (AR5). Climate models used in IPCC-AR5 are those of the Coupled Model Intercomparison Project phase 5 (CMIP5), in which the resolutions, parameterizations, and land cover in climate models are greatly improved [*Taylor et al.*, 2012]. *Cheng and Chiang* [2013] have used some CMIP5 models to study the AMOC variability in historical and global warming scenarios. In this paper, we examine the multidecadal variations of the AMOC and AMO in CMIP5 historical simulations. Our main objectives are to investigate the relationship between the multidecadal climate fluctuations of the AMOC and AMO and to identify possible physical mechanisms behind such a relationship.

[6] The paper is organized as follows. Section 2 briefly presents the modeling and observational data sets and statistical methods used in this study. The simulated AMOC and AMO variability in CMIP5 models is shown in section

3. Section 4 describes the potential relationship between the AMO and AMOC in CMIP5 models. Some discussions are given in section 5. The paper is concluded with a summary in section 6.

2. Data and Methods

[7] This study is based on 27 coupled GCMs output data of the “historical” simulations provided to the upcoming report of IPCC-AR5. The model data can be downloaded from the website of the Coupled Model Intercomparison Project phase 5 (CMIP5) [*Taylor et al.*, 2012] (<http://cmip-pcmdi.llnl.gov/cmip5/>). The purpose of these experiments is to address outstanding scientific questions that arose as part of the IPCC-AR4 assessment process, to improve understanding of climate, and to provide estimates of current and future climate change that will be useful to those considering its possible consequences. The historical run is forced by observed atmospheric composition changes which reflect both anthropogenic (such as green house gases and anthropogenic aerosols) and natural sources (volcanic influences, solar forcing, aerosols and emissions of short-lived species and their precursors) and, for the first time, including time-evolving land cover. These historical runs cover much of the industrial period from the mid-19th century to the present and are sometimes referred to as “20th century” simulations. The modeling center and country, IPCC model ID and temporal coverage for each model used in this study are shown in Table 1.

[8] Observational data set is used to validate the variability of coupled GCM simulations. SST data are from the monthly NOAA Extended Reconstruction Sea Surface Temperature version 3 (ERSST v3) [*Smith et al.*, 2008]. The temporal coverage is from January 1854 to the present and it has a spatial resolution on a 2° × 2° grid. The data can be obtained from <http://www.ncdc.noaa.gov/oa/climate/research/sst/ersstv3.php>.

[9] The AMO index is defined as the detrended area-weighted SST from the Atlantic western coast to the eastern coast and from 0°N to 60°N in both model output and ERSST data, which is similar to the definitions used in earlier studies [e.g., *Knight et al.*, 2005; *Sutton and Hodson*, 2005; *Trenberth and Shea*, 2006]. In models, the AMOC index is usually defined as the maximum AMOC stream function in a zonal band, either chosen at a specific latitude (usually 30°N) or in a latitude band (e.g., north of 20°N), measured in Sverdrup (1 Sv = 10⁶ m³ s⁻¹). Here we use both of the two definitions and find that their corresponding variations are very similar. To exclude or reduce surface wind driven overturning, we further use a criterion that the maximum stream function should be located deeper than 500 m [*Schott et al.*, 2004]. In this paper, the AMOC stream function is calculated from the meridional velocity $v(x, y, z, t)$ of the ocean products as:

$$\Psi(y, z, t) = \int_{-H}^{-z} \int_{x_{west}}^{x_{east}} v(x, y, z, t) dx dz,$$

where H is the sea bottom, x_{west} is the ocean western boundary, and x_{east} is the ocean eastern boundary.

Table 1. The 27 Models Involved in This Study and Their IPCC ID, Names, and the Temporal Coverage

Sponsor, Country	Model Name	Temporal Coverage
Commonwealth Scientific and Industrial Research Organisation (CSIRO), Australia	ACCESS1-0	1850.01–2005.12
Beijing Climate Center, China	bcc-csm1-1	1850.01–2012.12
Canadian Center for Climate Modeling and Analysis, Canada	CanESM2	1850.01–2005.12
National Center for Atmospheric Research (NCAR), USA	CCSM4	1850.01–2005.12
Météo-France/Centre National de Recherches Météorologiques, France	CNRM-CM5	1850.01–2005.12
Commonwealth Scientific and Industrial Research Organisation (CSIRO), Australia	CSIRO-Mk3-6-0	1850.01–2005.12
European Earth System Model, EU	EC-EARTH	1850.01–2009.12
Institute of Atmospheric Physics, Chinese Academy of Sciences, China	FGOALS-g2	1900.01–2005.12
U.S. Department of Commerce/National Oceanic and Atmospheric Administration (NOAA)/Geophysical Fluid Dynamics Laboratory (GFDL), USA	GFDL-CM3	1860.01–2005.12
	GFDL-ESM2G	1861.01–2005.12
	GFDL-ESM2M	1861.01–2005.12
National Aeronautics and Space Administration (NASA)/Goddard Institute for Space Studies (GISS), USA	GISS-E2-H	1850.01–2005.12
	GISS-E2-R	1850.01–2005.12
Met office Hadley Centre, UK	HadCM3	1859.12–2005.12
	HadGEM2-CC	1859.12–2005.11
	HadGEM2-ES	1859.12–2005.11
Institute for Numerical Mathematics, Russia	inmcm4	1850.01–2005.12
Institute Pierre Simon Laplace, France	IPSL-CM5A-LR	1850.01–2005.12
	IPSL-CM5A-MR	1850.01–2005.12
	IPSL-CM5B-LR	1850.01–2005.12
Center for Climate System Research (University of Tokyo), National Institute for Environmental Studies, and Frontier Research Center for Global Change (JAMSTEC), Japan	MIROC5	1850.01–2005.12
Max Planck Institute for Meteorology, Germany	MIROC-ESM	1850.01–2005.12
	MIROC-ESM-CHEM	1850.01–2005.12
	MPI-ESM-LR	1850.01–2005.12
	MPI-ESM-P	1850.01–2005.12
Meteorological Research Institute, Japan	MRI-CGCM3	1850.01–2005.12
Norwegian Climate Centre, Norway	NorESM1-M	1850.01–2005.12

[10] Several statistical methods are used in this study, including the autocorrelation, lead-lag cross correlation, multitaper power spectrum [Mann and Lees, 1996], and maximum covariance analysis (MCA) [Czaja and Frankignoul, 2002; Rodwell and Folland, 2003; Gastineau and Frankignoul, 2012; Gastineau et al., 2013]. The MCA is a useful tool to investigate the relationship of two variables as a function of time lag. For detail of the MCA method, see Czaja and Frankignoul [2002]. Only the first mode of the MCA will be discussed here since no significant relation was found in higher modes. The statistical significance of the correlation (squared covariance fraction) is assessed with a Monte Carlo approach by comparing the correlation (squared covariance fraction) to that of a randomly scrambled field. We randomly permute the SST (or the AMOC) time series by blocks of 1 year, and perform an MCA. We repeat this analysis 100 times. The estimated significance level is percentage of randomized correlation (squared covariance fraction) that exceeds the correlation being tested. It is an estimate of the risk of rejecting the null hypothesis (no relationship between two variables, squared covariance fraction is zero), and a smaller significance level indicates the presence of stronger evidence against the null hypothesis.

[11] To investigate statistical significance of the lagged correlation, we calculate the effective degree of freedom as follows:

$$F = N \times (1 - r_1 \times r_2) / (1 + r_1 \times r_2),$$

where N is the length of data, r_1 and r_2 are the autocorrelation with the lag of one time step for variables 1 and 2, respectively [Bretherton et al., 1999]. The seasonal cycle and the linear trend in the time series are removed from the monthly values prior to the analysis. In order to remove high frequency variability, time series are filtered using a 15 year low-pass filter when it is necessary. Note that the results are not sensitive to the cutoff frequency when we choose other low-pass frequency bands from 8 to 15 years (not shown).

3. Simulated AMO and AMOC Variability in CMIP5 Models

3.1. The AMO

[12] The detrended annual mean AMO index for the different models and ERSST data are shown in Figure 1. The AMO index has been subtracted by the long-term mean and smoothed by a 15 year low-pass filter. The individual models (color lines) show highly varying amplitudes and various phases, with a large spread of uncertainty. However, all models do display a warming in the last two decades when anthropogenic warming becomes influential. In comparison with the observation (thick black line), the CMIP5 model ensemble mean (dash black line) shows much less variability, particularly in the period from 1890 to 1960. This is to be expected from an average of many independent realizations. There is an exception from 1995 to the present during which the model ensemble mean coincides well with the

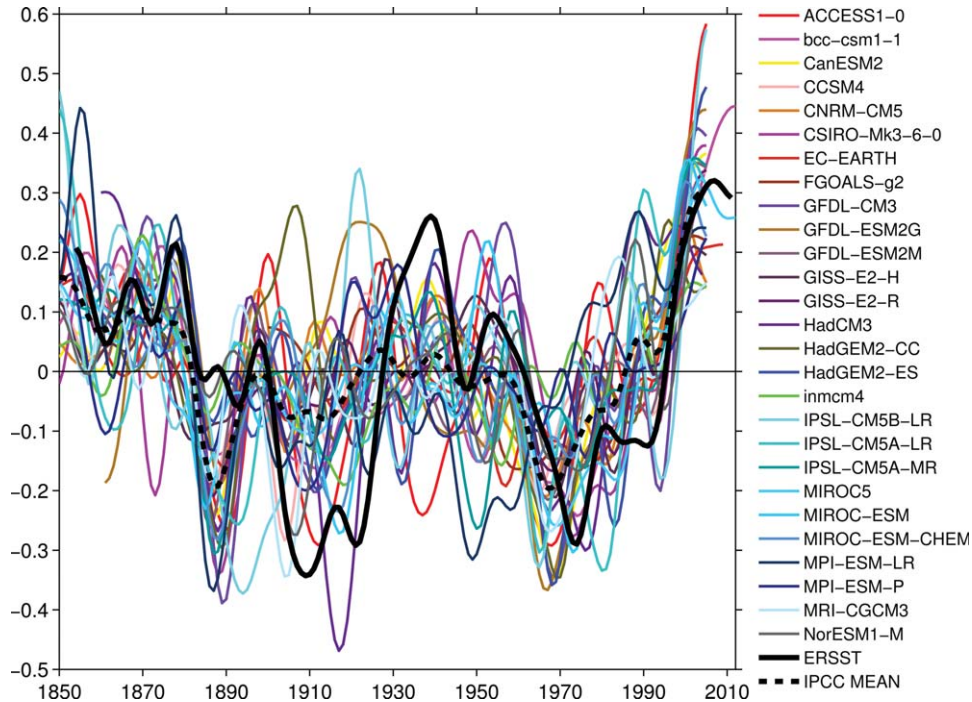


Figure 1. The annual mean AMO index in CMIP5 historical simulations (thin color lines) and ERSST observation (thick black line). Unit is °C. The black dash line represents the ensemble mean of all CMIP5 models. All curves are detrended and are smoothed by a 15 year low pass filter.

observation. A close examination finds that the two main discrepancies between the model spread and the observation are during the early 20th century (1900–1925) when the models underestimate the cooling and during the subsequent warm period (1926–1965) when the models are generally too cool. The inconsistencies could arise from errors in the observed time series, inadequacy in the modeled response to the external and/or internal forcing, or the different phases of natural variability in different models. Compared to the CMIP3 model simulation of the AMO [Medhaug and Furevik, 2011; Ting et al., 2009, 2011], the behavior of the AMO in CMIP5 generally becomes better, particularly after 1960. This may be due to the high-resolution, improved parameterizations and the added time-evolving land cover modules in CMIP5 models. In addition to the amplitude and phase of the AMO index, we also examine the root-mean-square values (or standard deviation) of the AMO time series, as exhibited in Figure 2. The amplitudes of the AMO variability in CMIP5 models are comparable to, or slightly weaker than observed one with typical amplitudes ranging from 0.09°C to 0.19°C as compared to about 0.175°C in the 20th Century observation. It is also found that the AMO standard deviation in CMIP5 models is much larger than that in CMIP3 shown by Ting et al. [2011] and thus is more close to the observation, suggesting that CMIP5 models have been improved a lot compared to CMIP3 at least in simulating the AMO.

[13] To assess and compare the temporal variations of the AMO, we calculate and compare the lagged autocorrelations of the AMO index for each CMIP5 model for lags from 0 to 35 years (Figure 3). The autocorrelation function of the ERSST AMO is shown as the solid black line and behaves similarly to a perfect sinusoidal function with a

period of about 70 years, indicating the quasi-periodic nature of the observed AMO. For models, in addition to the longer than 50 year variations, most of them also have the relatively short periods of oscillation from 20 to 35 years, which can also be seen from the spectrum analysis (Figure 4). The persistence in the AMO index is defined as the

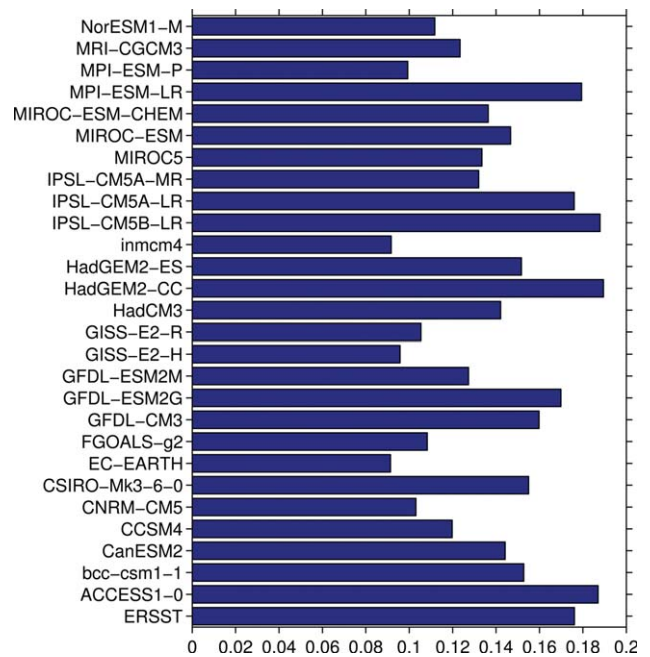


Figure 2. The corresponding amplitude (standard deviation) for the AMO index shown in Figure 1.

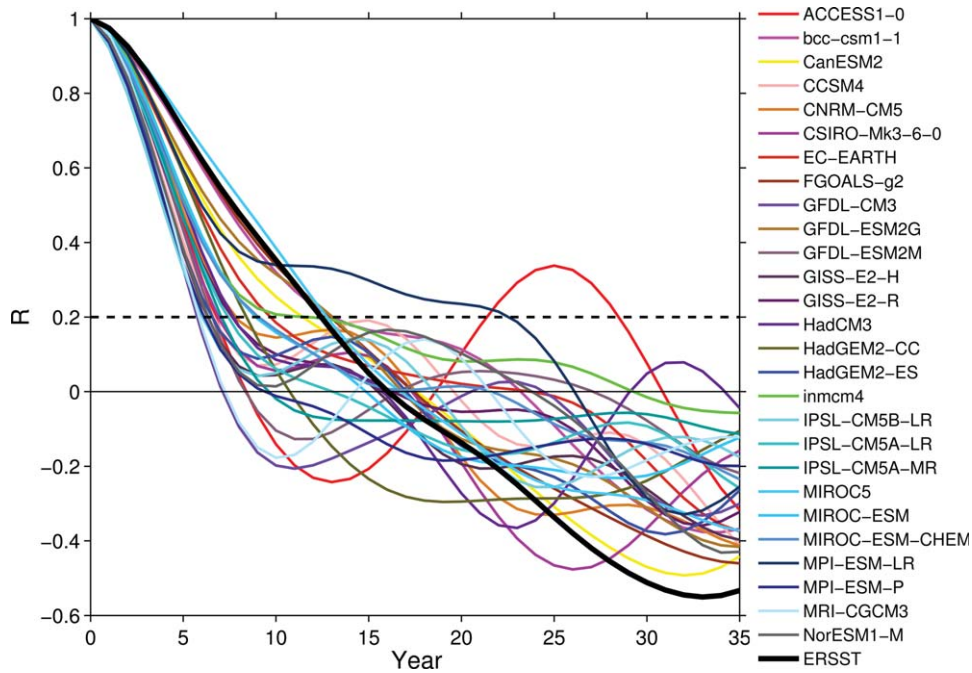


Figure 3. Autocorrelation of the AMO index in CMIP5 models (color lines) and observation (thick black line) with lags from 0 to 35 years. The dash line indicates the 80% confidence level for the observed AMO.

maximum time lag when the autocorrelation first crosses the significance line at the 80% level (Figure 3). A close inspection finds that the model persistence varies from 5 and up to 22 years, implying the potential for predicting future SSTs. However, for most of models the persistence is shorter than that of observation (the persistence of

ERSST is about 12 years). Meanwhile, the AMO persistence in CMIP5 is much longer than that in CMIP3 which shows an averaged persistence about 5 years [Medhaug and Furevik, 2011]. Figure 4 shows the power spectrum of the detrended annual mean AMO index. ERSST primarily has three peaks of energy spectrum around 40 years, 25 years,

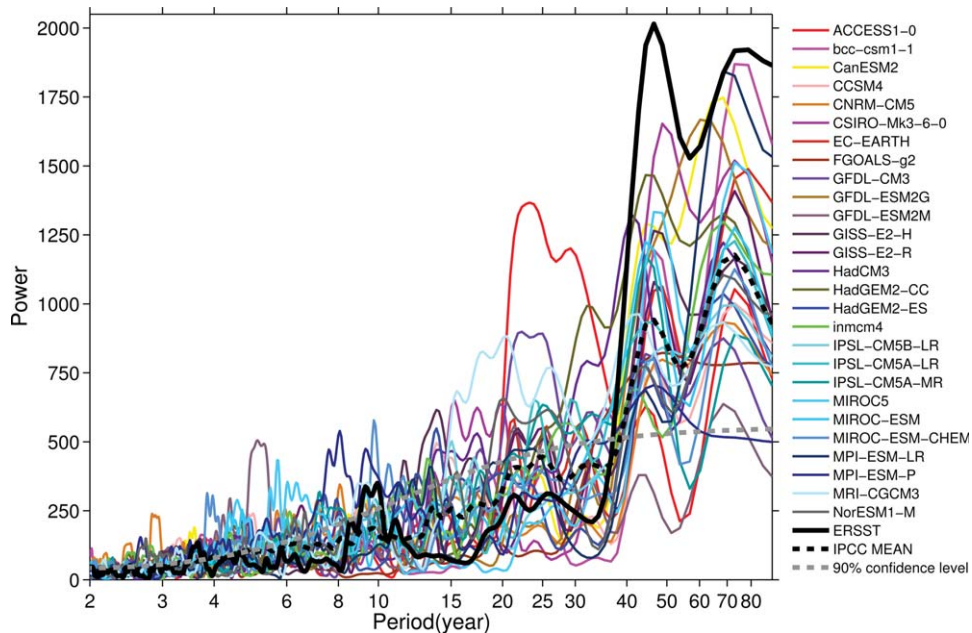


Figure 4. Power spectrum of the annual mean AMO index in CMIP5 historical simulations (color lines) and in observation (thick black line). The time series are linear detrended but not filtered. The dash line represents the ensemble mean of the power spectrum in all CMIP5 models. The dash gray line denotes the 90% confidence red noise spectrum.

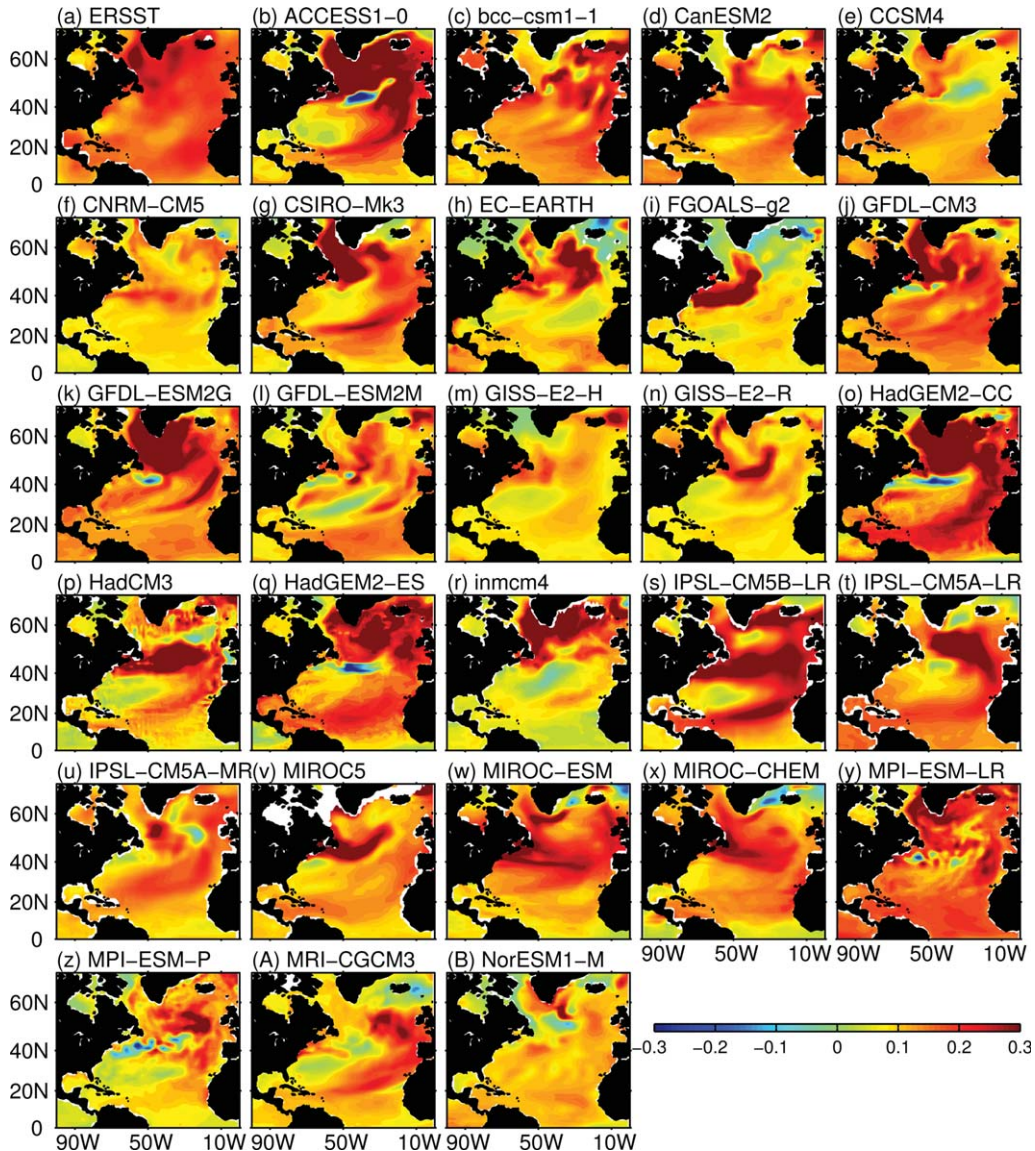


Figure 5. Regression of the North Atlantic SST on the normalized AMO index for (a) observation and (b–B) CMIP5 historical simulations. Unit is $^{\circ}\text{C}$.

and 10 years. Most models display the maximum power at multidecadal time scales (above 40 years) but with too weak amplitudes compared to the observation. On the other hand, the power spectrum peaked at the band of 20–30 years features more energy than the observation, as shown in the ensemble mean result in Figure 4. Furthermore, most of models underestimate or even do not capture the 10 years peak. Generally speaking, the temporal properties of the AMO in CMIP5 models are closer to the observation than those in CMIP3 [Medhaug and Furevik, 2011; Ting *et al.*, 2011].

[14] The spatial structures of the AMO in both models and observation are determined by linearly regressing the grid point SST onto the AMO index (Figure 5). The positive phase of the observed AMO is characterized by a comma-shaped SST pattern in the North Atlantic with the largest amplitude over the subpolar regions and an extension along the east side of the basin and into the subtropical North Atlantic (Figure 5a). Most of the CMIP5 model sim-

ulations have reproduced the AMO pattern (Figure 5b–B) with a similar shaped SST pattern in the North Atlantic. The amplitude of warming (cooling) during the AMO warm (cold) phase in most of models is slightly weaker than in observations, particularly in the tropics. It is also found that in some models such as CNRM-CM5, CanESM2, HadCM3, MIROC5, and MIROC-CHEM, the largest SST anomaly is not over the subpolar region but shifts a little bit to the south. Observation shows a reduced magnitude of SST anomaly in the Gulf Stream area and in the Nordic Seas. Most models also simulate reduced or slightly cooling (warming) during AMO warm (cold) phase along these regions, but for some models the region is shifted slightly north or is distributed over a larger area.

3.2. The AMOC

[15] The long-term mean structures of the AMOC in 18 CMIP5 models are shown in Figure 6. All models generally capture the basic structure of the AMOC, with a warm

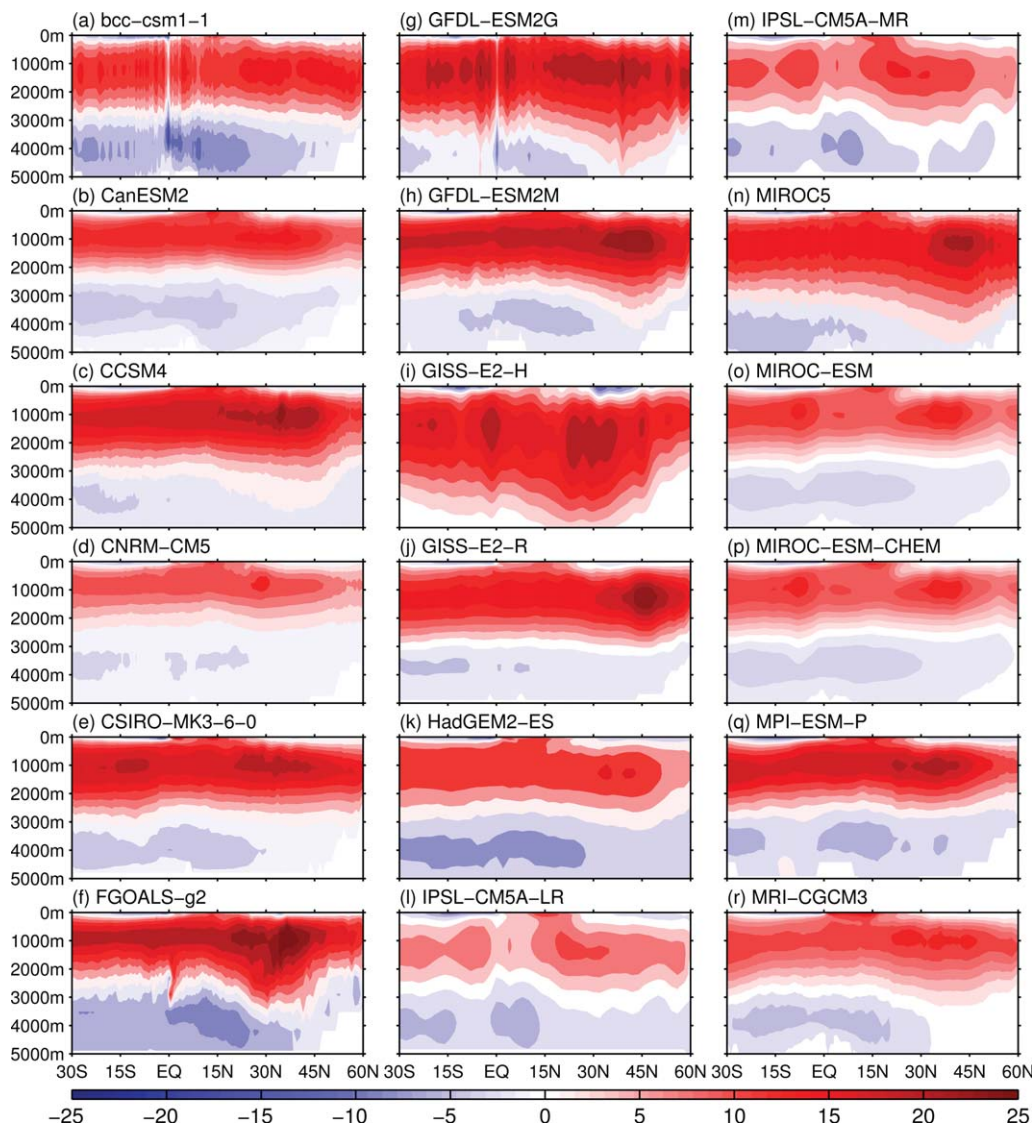


Figure 6. Long-term mean zonal integrated AMOC stream function in CMIP5 historical simulations. Unit is Sv.

northward current in the upper layer (upper 1000 m) and a cold southward current in the low layer (2000–3000 m). There is an exception in GISS-E2-H model in which the low branch of the AMOC can penetrate to the bottom of the basin to 5000 m (Figure 6i). This leads to a disappearance of the lower overturning cell called the Antarctic Bottom Water (AABW) cell. GISS-E2-H is the only model which is not able to simulate the AABW cell, while the other models can reproduce this low cell although the strength and location of the low cell may be different from observation [Johnson, 2008]. Some of the models show that the AABW cell has almost disappeared north of 35°N which is consistent with observation [Johnson, 2008], whereas other models show the AABW cell all the way north to 60°N.

[16] It is seen that the position of the maximum AMOC transport occurs at 500–1500 m depth and between 20°N and 60°N. Therefore, we choose the maximum stream function between 20°N and 60°N and below 500 m as the index for the AMOC. Similar results can be obtained if we

choose the AMOC index as the maximum stream function at 30°N (not shown). The models show a long-term mean overturning circulation range from 13 Sv to 31 Sv, as displayed in Figures 6 and 7. Compared to the observed AMOC strength that roughly in a range of 13–24.3 Sv [Ganachaud and Wunsch, 2000; Lumpkin and Speer, 2003; Ganachaud, 2003; Smethie and Fine, 2001; Talley et al., 2003; Cunningham et al., 2007], FGOALS-g2 and GISS-E2-R models seem to overestimate the strength of the AMOC. The ensemble mean strength of the AMOC is about 20 Sv (Figure 7), which is in the range of observation. Compared with the CMIP3 models as shown in Medhaug and Furevik [2011], the strength of the AMOC in CMIP5 is generally more reasonable and is closer to the observations.

[17] In addition to the long-term mean structures, the AMOC exhibits a low-frequency variability among CMIP5 models. Figure 7 shows the time series of AMOC indices during the 20th Century. All models display distinct decadal or multidecadal fluctuations. This can also be seen from

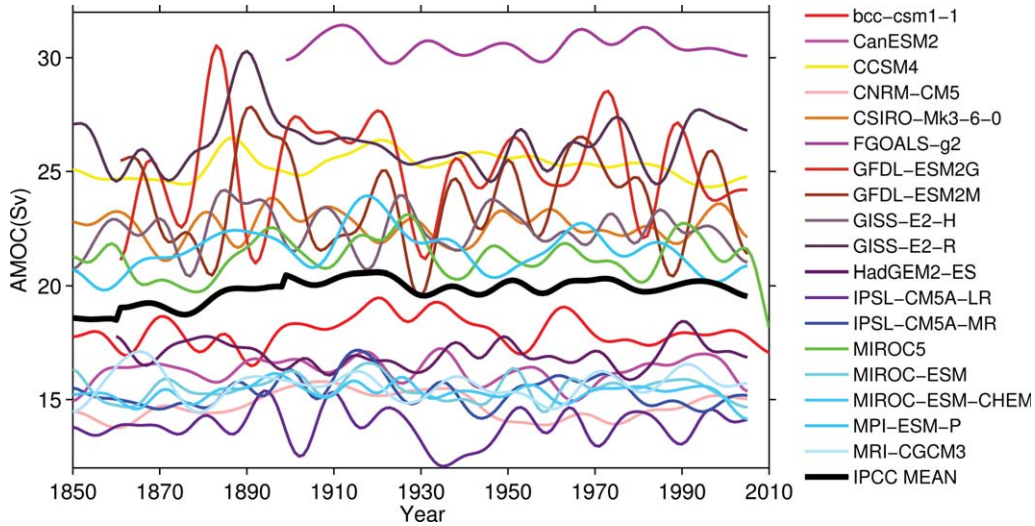


Figure 7. The AMOC index for individual models (color lines) and ensemble mean result (thick black line), defined as the maximum stream function north of 20°N and below 500 m depth. All curves are detrended and smoothed by a 15 year low frequency filter. Unit is Sv.

the autocorrelation and spectrum analysis (Figures 8 and 9). The models have the largest energy on multidecadal timescales, particularly at period longer than 30 years. For the period between 15 and 30 years, the energy is of secondary importance (Figure 9). Autocorrelation also displays that the AMOC index does not have a single well-defined periodicity but varies across a range of decadal or multidecadal timescales (Figure 8). For the individual model, the persistence in the AMOC variability varies from 6 to 18 years (Figure 8), defined as the maximum time lag when the autocorrelation first crosses the significance line at the 80% confidence level.

4. Relationship Between the AMOC and AMO

4.1. Lead-Lag Correlations of the AMO and AMOC

[18] To examine the relationship between the AMOC and AMO, we first calculate the lead-lag correlations

between the two indices (Figure 10). It can be seen that the lead-lag correlations show highly varying patterns among 18 CMIP5 models. A close inspection finds that the relationship between the AMOC and AMO in most models is characterized by a positive correlation when the AMOC leads the AMO and a negative correlation when the AMO leads the AMOC. These models include CanESM2, CNRM-CM5, CSIRO-MK3-6-0, GFDL-ESM2G, GFDL-ESM2M, GISS-E2-H, GISS-E2-R, MIROC5, MIROC-ESM-CHEM, and MPI-ESM-P (Figures 10a–10j). When the AMOC leads the AMO, a strengthened (weakened) AMOC produces a heat transport convergence (divergence) in the North Atlantic Ocean and thus generates a warm (cool) phase of the AMO. After some time delay, the warm (cool) phase of the AMO tends to reduce (enhance) the meridional density gradient over the North Atlantic Ocean, which weakens the original AMOC anomaly and eventually leads to a weakening (strengthening) of the AMOC.

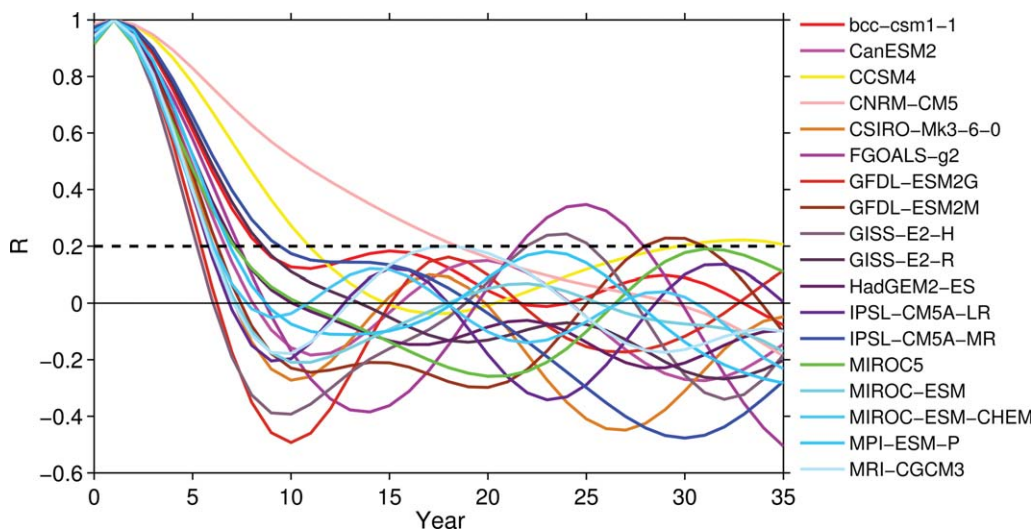


Figure 8. Same as Figure 3 but for the AMOC index.

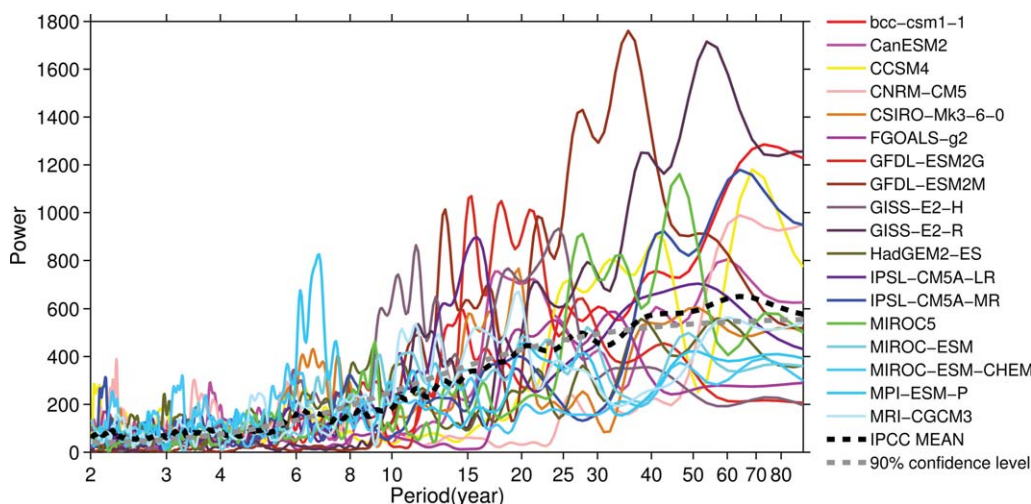


Figure 9. Same as Figure 4 but for the AMOC index.

After ocean adjustments, the new AMOC anomaly is in favor of generating an anomalous AMO which will further feedback to the AMOC a few years later. The same processes repeat and repeat. The AMOC system eventually oscillates on multidecadal timescales. The key elements in this oscillation are the slow adjustment of ocean circulation and the associated time delay in the advective flux response to a change in the meridional density gradient, which provide both the positive and negative feedbacks to the entire system. This relationship is consistent with the delayed advective oscillation mechanism of the AMOC proposed by *Lee and Wang* [2010]. Here, the temperature variation is an important factor to control the density change [e.g., *Wang et al.*, 2010]. Furthermore, it is worth noting that the lead (positive correlation) and lag (negative correlation) times vary for each model. This may be associated with the time-scale of ocean adjustment that depends on density anomaly induced by both temperature and salinity, or the locations of convective activity which are not simulated correctly in some of CMIP5 models.

[19] Additionally, the correlation between the AMOC and AMO can also be a uniformly positive or negative value in both lead and lag. For example, HadGEM2-ES model features a positive correlation regardless of lead and lag, with a strengthened AMOC coinciding with a warm AMO phase and vice versa. This suggests that there is a positive feedback between the AMOC and AMO. If there are no other feedbacks, the AMOC and AMO will not oscillate. Similarly, a negative correlation prevails in CCSM4 model no matter when the AMOC leads or lags the AMO.

[20] The relationship between the AMOC and AMO can be further revealed by the lead-lag correlation of the AMO with the AMOC at each latitude (Figure 11). Here, the AMOC index in each latitude is defined as the maximum of the zonal integrated stream function in depth space. As expected, the correlation in Figure 11 north of 20°N is quite similar to Figure 10. It is interesting to find that the AMOC lead and lag times in the correlation maps are large in high latitudes and decrease southward in most of the coupled models. This mainly arises from the latitudinal dependence of the AMOC variations suggested by *Zhang* [2010]. Based

on the GFDL-CM2.1 model, *Zhang* [2010] argued that the subpolar AMOC variations lead the subtropical and tropical AMOC variations by several years (about 5 years) and the length of time lag is mainly determined by the advection speed in the North Atlantic deep water formation region.

[21] Two models of bcc-csm1-1 and IPSL-CM5A-MR are different and complicated. In these two models, the correlation exhibits a discontinuity as the latitude is changed. Moreover, the lead-lag correlation south of 20°N is quite different from that north of 20°N in these two models. Therefore, we exclude them in the following discussion.

[22] Based on the lead-lag correlations in Figures 10 and 11, we separate all models into four categories (Table 2). In Category I, 11 models are featured by a delayed advective oscillator with a positive (negative) correlation when the AMOC leads (lags) the AMO: CanESM2, CNRM-CM5, CSIRO-MK3-6-0, GFDL-ESM2G, GFDL-ESM2M, GISS-E2-H, GISS-E2-R, MIROC5, MIROC-ESM-CHEM, MPI-ESM-P, and IPSL-CM5A-LR. Note that IPSL-CM5A-LR is included in Category I because of its correlation map in Figure 11k (although Figure 10k does not show an obvious positive (negative) lead (lag) correlation like other models). In Category II, 3 models mainly display a significantly negative correlation no matter when the AMOC leads or lags: CCSM4, MIROC-ESM, and FGOALS-g2. In Category III, 2 models primarily exhibit a significantly positive correlation regardless of the AMOC lead or lag: HadGEM2-ES and MRI-CGCM3. Finally, in Category IV, 2 models display a complicated correlation between the AMO and AMOC: bcc-csm1-1 and IPSL-CM5A-MR.

4.2. Maximum Covariance Analysis of the North Atlantic SST and AMOC Stream Function

[23] We use the Maximum Covariance Analysis (MCA) to investigate how the AMOC is related to the North Atlantic SST in lead and lag conditions. Lagged covariance is powerful in distinguishing between cause and effect in the relationship between the AMOC and AMO. On annual or longer timescales, the AMO is usually regarded as a passive response to the AMOC [*Delworth and Mann*, 2000; *Knight et al.*, 2005; *Medhaug and Furevik*, 2011]. If the AMO only responds passively, there should be no

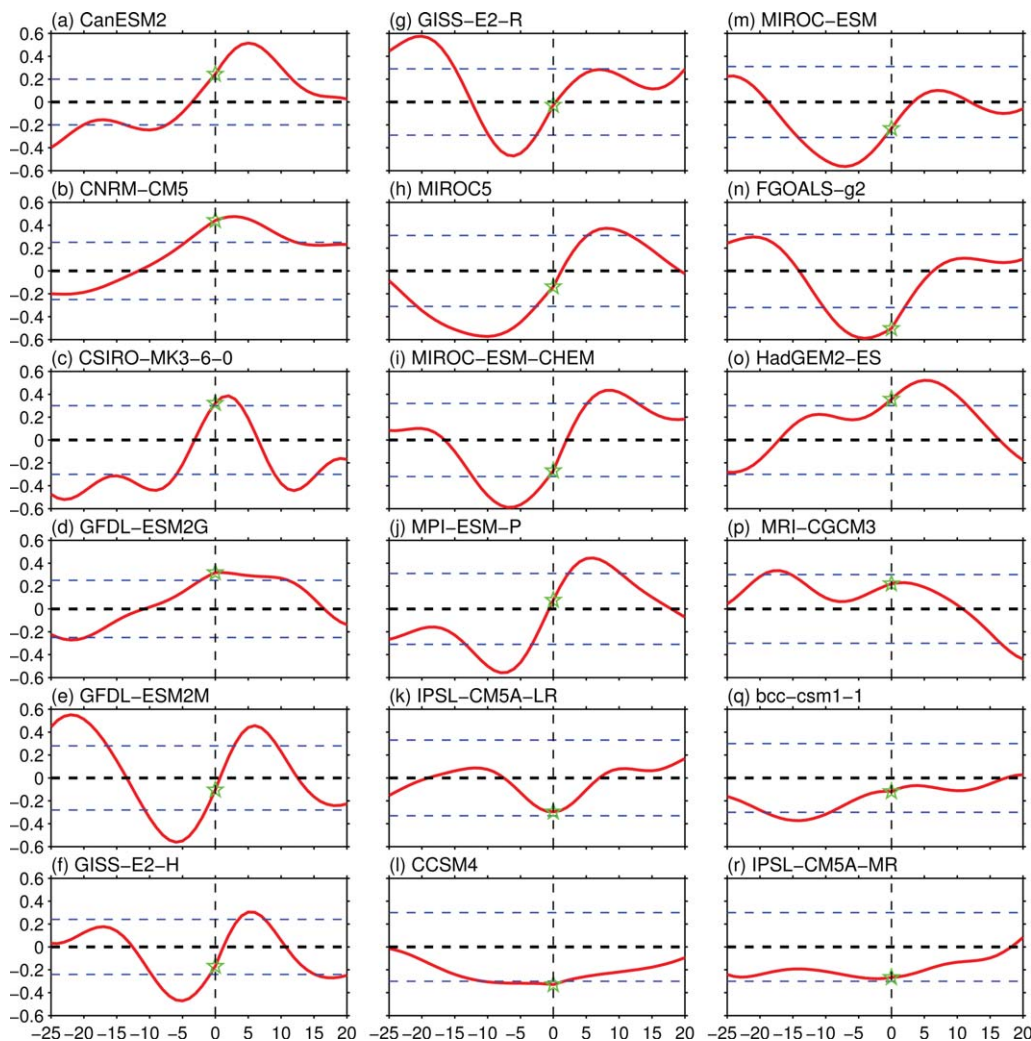


Figure 10. Lead-lag correlation between the AMO and the AMOC indices in CMIP5 historical simulations. The unit of value in x axis is year. Positive (negative) years in x axis mean the AMOC leads (lags) the AMO. The dash lines are the 80% confidence level.

significant covariance when the AMO leads the AMOC. If the AMO fluctuations influence the AMOC, their cross-covariance does not vanish when the AMO leads. Such signatures are searched and evaluated in CMIP5 models here by applying the MCA between the AMO and AMOC as a function of time lags. All fields are normalized and smoothed by a 15 year filter.

[24] First, we explore the behavior of Category I models by using the MCA method. The GFDL-ESM2M model is taken as an example. Figure 12 shows the AMOC stream function and North Atlantic SST covariance maps of the first MCA mode from lag -6 to 10 years. The correlation coefficient r between the AMOC stream function and North Atlantic SST time series and the squared covariance fraction F of the mode are also given for each lag. The correlation r has a pronounced positive value when the AMOC stream function leads the North Atlantic SST, reflecting that the SST can be a response to the AMOC variations. When the AMOC leads by 1–6 year or in phase with the North Atlantic SST, we recover the strengthened AMOC pattern associated with the warm AMO phase (Figures 12a–12c) [Enfield *et al.*, 2001; Knight *et al.*, 2005]. The

former acts as a driver, primarily through anomalous heat transport convergence or divergence in the North Atlantic Ocean as documented in various studies [e.g., Delworth and Mann, 2000; Delworth *et al.*, 1993; Knight *et al.*, 2005; Knight, 2009]. This AMO response to the AMOC is thus usually regarded as the zero-order description of the interaction between the AMOC and AMO. Figure 12 nevertheless indicates that significant covariance is also found when the SST leads the AMOC stream function by several years. As seen in Figures 12d–12e, the correlation between the AMOC stream function and the SST time series can be as large as 0.77. Accordingly, we recover a good correspondence between the warm phase of the AMO and the weakened AMOC spatial pattern. Preceding a negative AMOC anomaly, there is a warm SST anomaly over the subpolar region, extending southwestward to the tropical North Atlantic, which is a typical AMO warm phase in GEDL-ESM2M model as shown in Figure 51. That indicates that the AMO is not only passively responded to the AMOC but also can drive the AMOC variations. The impact of the AMO on the AMOC is expected to be largely associated with the temperature induced meridional density

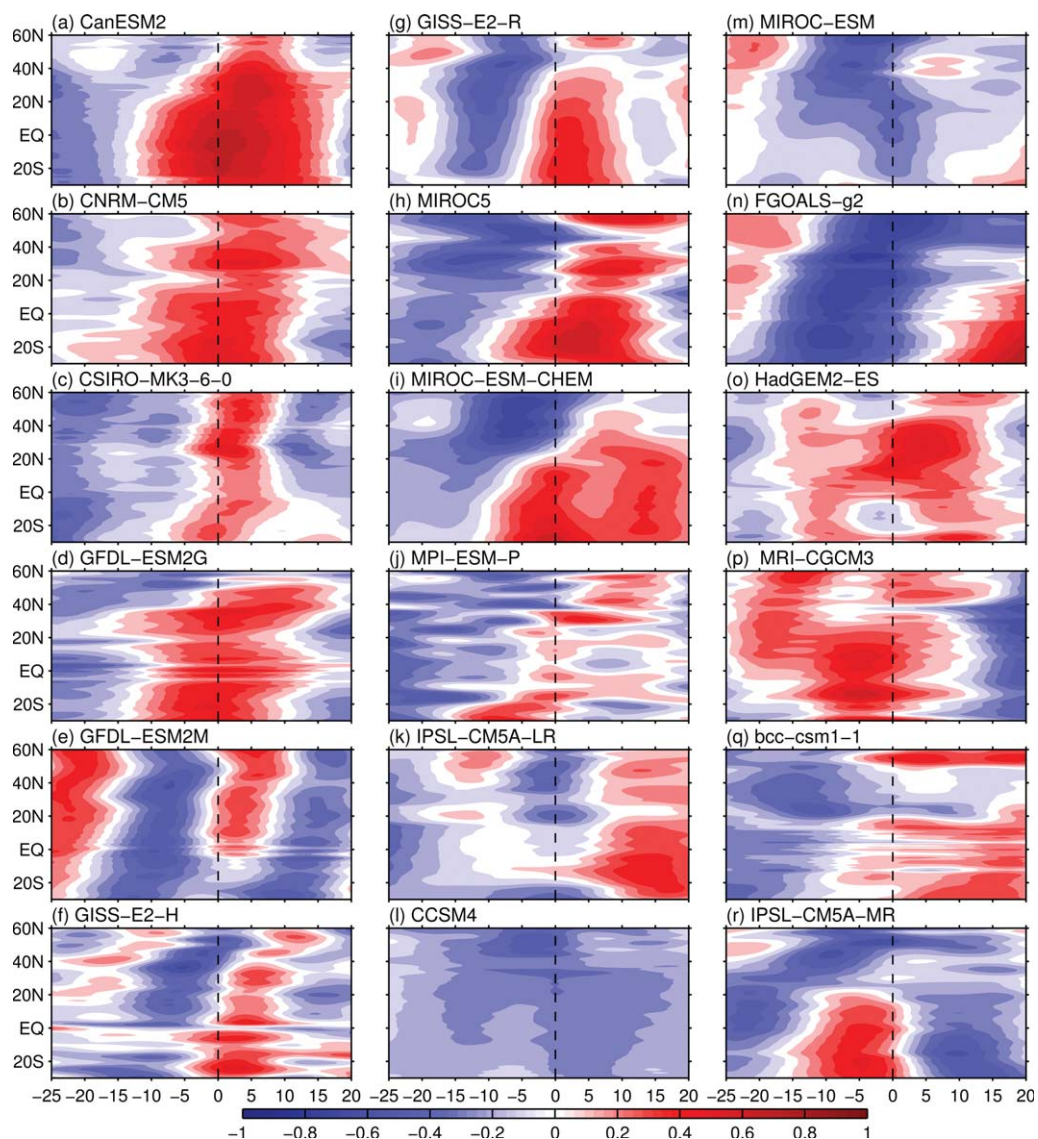


Figure 11. Lead-lag correlation between the AMO and the AMOC indices at each latitude in CMIP5 historical simulations. The AMOC index at each latitude is defined as the maximum stream function below 500 m. The unit of value in x axis is year. Positive (negative) years in x axis mean the AMOC leads (lags) the AMO.

gradient, as suggested and shown by *Lee and Wang* [2010] and *Wang et al.* [2010]. The warm AMO phase with a warmer SST in the high latitude and a relatively

colder SST in the subtropics is in favor of generating a decreased meridional density gradient, which in turn leads to a weakened AMOC. These results are consistent

Table 2. Four Groups of Models Categorized Based on Performance Shown in the Lead-Lag Correlation Between the AMOC and AMO

Category	Description	Models
I	AMOC leads AMO: positive correlation AMOC lags AMO: negative correlation	CanESM2, CNRM-CM5, CSIRO-MK3-6-0, GFDL-ESM2G, GFDL-ESM2M, GISS-E2-H, GISS-E2-R, MIROC5, MIROC-ESM-CHEM, MPI-ESM-P, IPSL-CM5A-LR
II	AMOC leads AMO: negative correlation AMOC lags AMO: negative correlation	CCSM4, MIROC-ESM, FGOALS-g2
III	AMOC leads AMO: positive correlation AMOC lags AMO: positive correlation	HadGEM2-ES, MRI-CGCM3
IV	AMOC leads AMO: complicated AMOC lags AMO: complicated	Bcc-csm1-1, IPSL-CM5A-MR

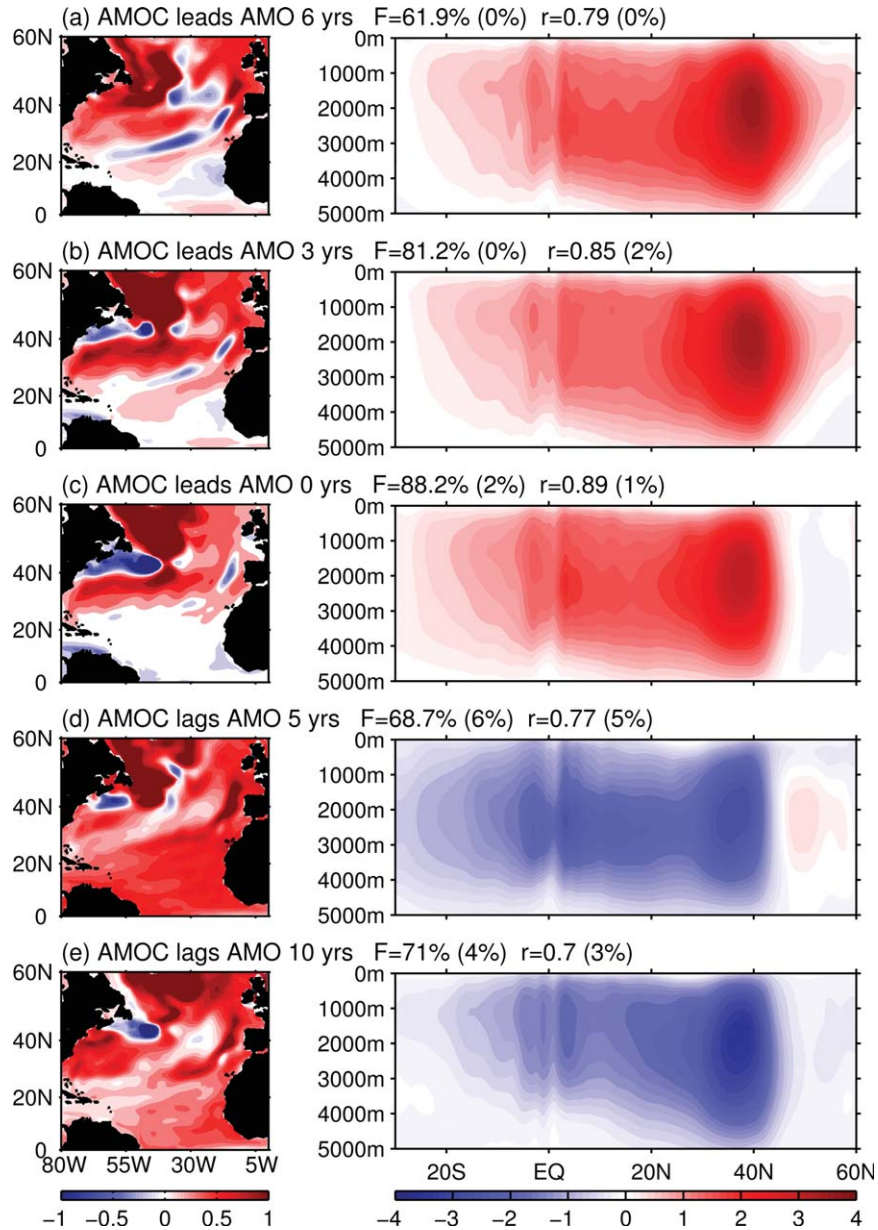


Figure 12. (a–c) Homogeneous AMOC and heterogeneous SST covariance maps for the first MCA mode between the Northern Atlantic SST and the AMOC stream function anomalies in Category I GFDL-ESM2M model. (d–e) same as Figures 12a and 12b but for the homogeneous SST and heterogeneous AMOC covariance maps. The results are shown from lags -6 to 10 years. The correlation coefficient r between the SST and AMOC MCA time series, and the squared covariance fraction F of the mode are given for each lag. The percentages in parentheses give the corresponding estimated significance level for F and r .

with the lead-lag correlation analysis shown in Figures 10e and 11e.

[25] Similar features can be found in other models of Category I. Figures 13 and 14 show the first MCA modes of the North Atlantic SST and the AMOC stream function at selected leads (left figures) and lags (right figures) in the other models of Category I. We choose these lead and lag years because the first MCA mode at these years can typically represent the characteristics of the AMO and AMOC and are statistically significant. At other leads and lags, the pattern and phase are quite similar but with a different

amplitude. It is seen that all Category I models experience a warm AMO phase after a strengthening of the AMOC. This relationship peaks at different lead years which can range from 0 to 9 years and account for different percentages of the total covariance (F : 48.1–94.3%) in different models. The AMO signal extracted from the first MCA mode between the SST and AMOC varies from model to model, as exhibited in Figures 12–14. This is not surprising since the AMO has different manifestations in different models. A close examination can be found that the extracted AMO spatial pattern from the MCA is consistent

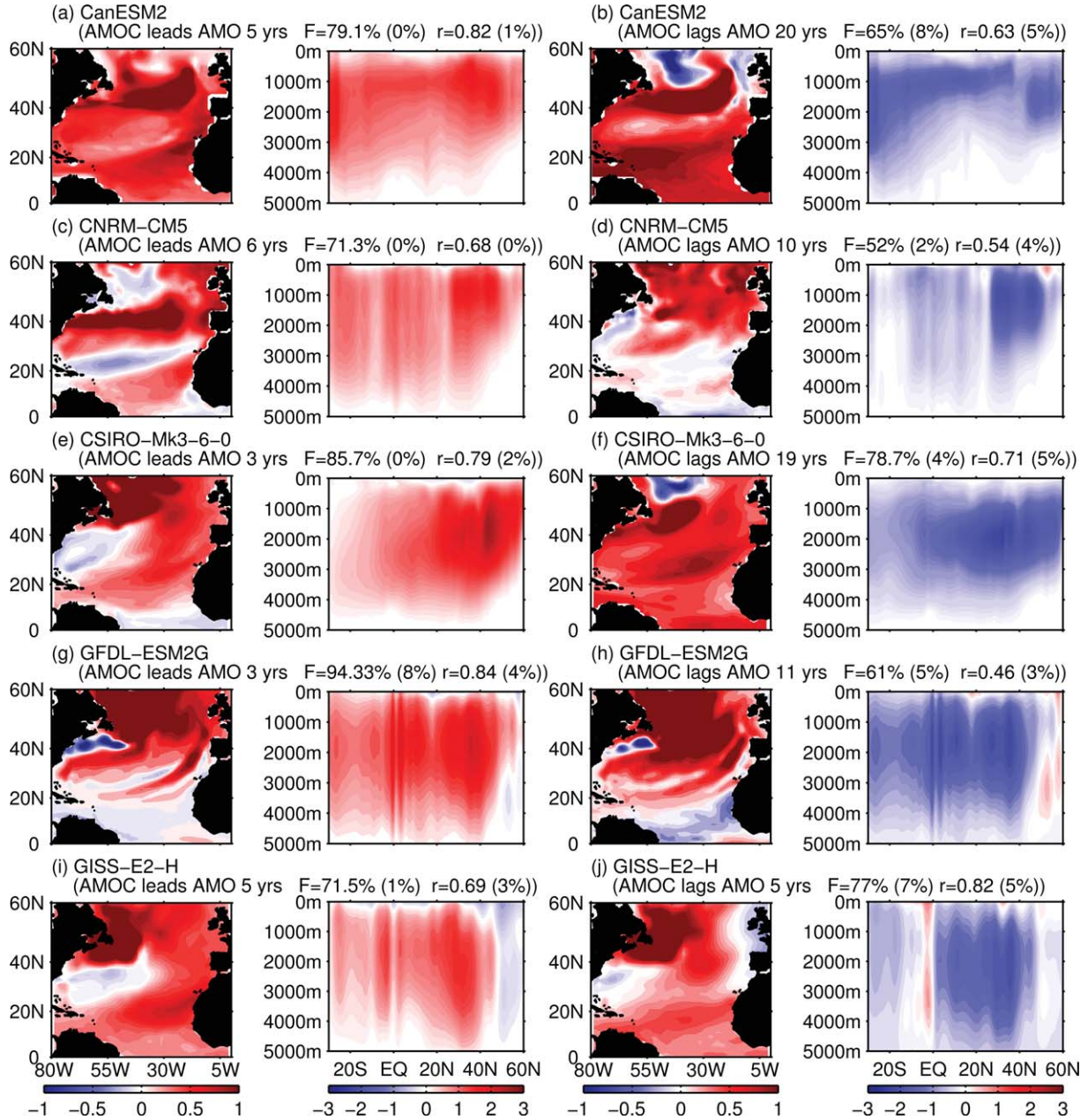


Figure 13. Same as Figure 12 but for the Category I CanESM2, CNRM-CM5, CSIRO-MK3-6-0, GFDL-ESM2G, and GISS-E2-H models at selected leads (homogeneous AMOC and heterogeneous SST maps in left two figures) and lags (homogeneous SST and heterogeneous AMOC maps in right two figures).

with the AMO pattern shown in Figure 5 for each model. On the other hand, all Category I models present a warm AMO phase preceding a weakened AMOC. This is to be expected as the meridional density gradient decreases during the AMO warm phase. In general, the relationship between the AMO and AMOC in Category I models resembles the delayed advective oscillation with a positive correlation when the AMOC leads the AMO and a negative correlation when the AMO leads the AMOC. Due to the slow adjustment of ocean circulation response to the density variations, the AMOC and AMO can oscillate on multidecadal timescales.

[26] In Category II models, the MCA of the North Atlantic SST and AMOC stream function exhibits a consistent result with the lead-lag correlation shown in section 4.1. As displayed in Figure 15, we take FGOALS-g2 model as an example. It can be seen that the correlation between the SST and AMOC time series extracted from the first MCA mode presents high values in both lead and lag. Further inspection finds that the associated spatial pattern in both lead and lag shares great similarities, with a warm AMO phase coinciding with a weakened AMOC strength. That indicates a weakened (strengthened) AMOC can generate a warm (cold) phase of the AMO which

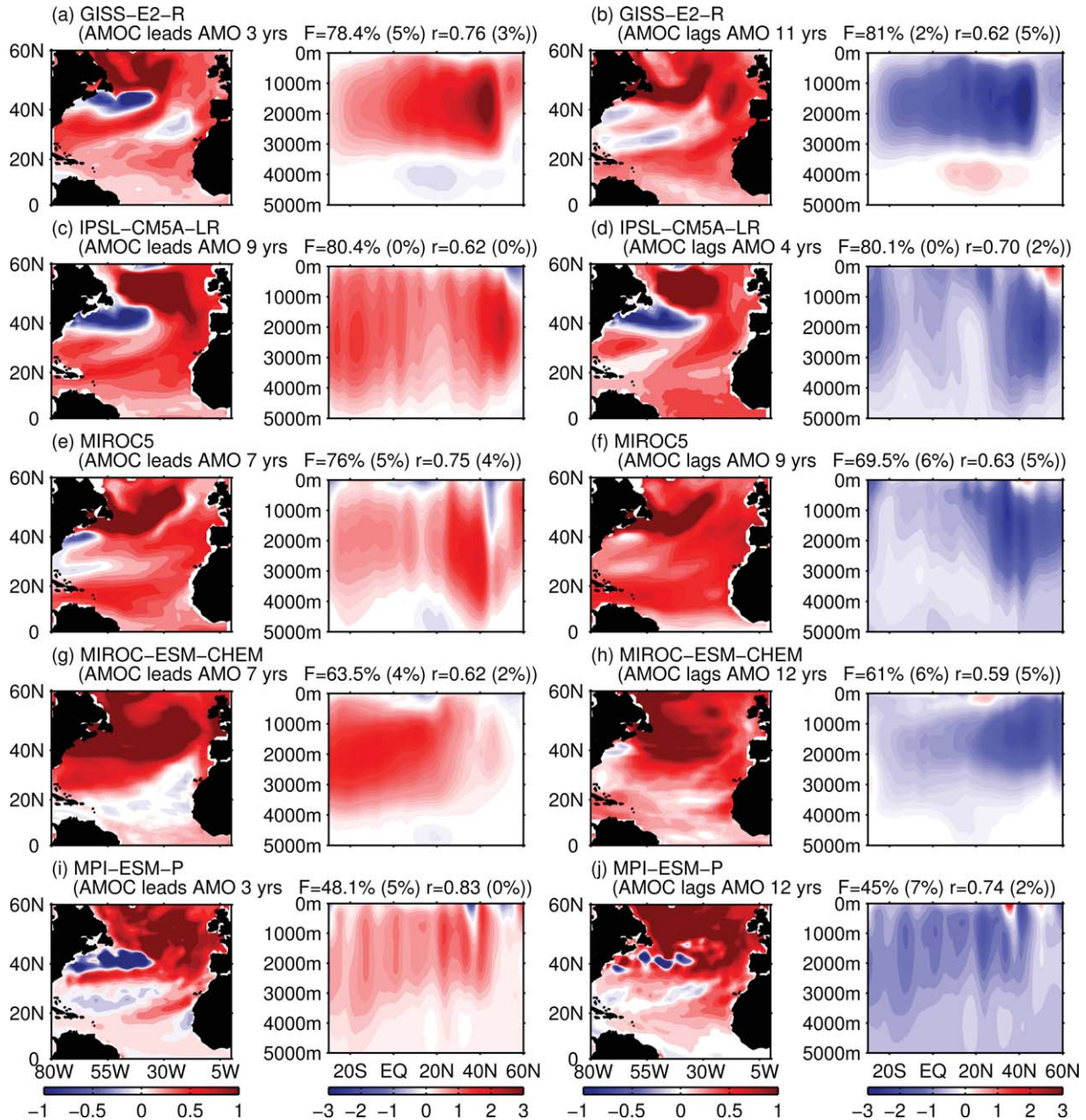


Figure 14. Same as Figure 13 but for the Category I GISS-E2-R, IPSL-CM5A-LR, MIROC5, MIROC-ESM-CHEM, and MPI-ESM-P models at selected leads and lags.

inversely leads to a further weakening (strengthening) of the AMOC after some ocean adjustment. This positive feedback can damp or infinitely amplify the AMOC strength, which in turn should lead to a collapse or extremely large value of the AMOC if there are no other feedbacks and processes. It is not easy to understand why the weakened AMOC can lead to a warm phase of the AMO. This may arise from that the AMO is not determined only by the AMOC-induced heat transport convergence and other factors may dominate the AMO variability in coupled models. Similar behaviors can be obtained from the other models in Category II (MIROC-ESM and CCSM4). Figure 16 shows the first MCA mode of the North Atlantic SST and the AMOC stream function

at selected lead and lag times in MIROC-ESM and CCSM4 models. Regardless of lead and lag, the warm phase of the AMO is associated with a weakened AMOC. Both of them are consistent with the lead-lag correlations shown in Figures 10 and 11.

[27] In contrast to Category I and II models, the relationship between the AMOC and AMO in Category III models is quite different. As seen in Figure 17, the first MCA mode in different lead and lag times basically show a warm phase of the AMO corresponding to a strengthening of the AMOC. This indicates that the AMO is passively responded to the AMOC when the AMOC leads on one hand, and the warm (cold) phase of the AMO can result in a strengthened (weakened) AMOC on the other hand. The

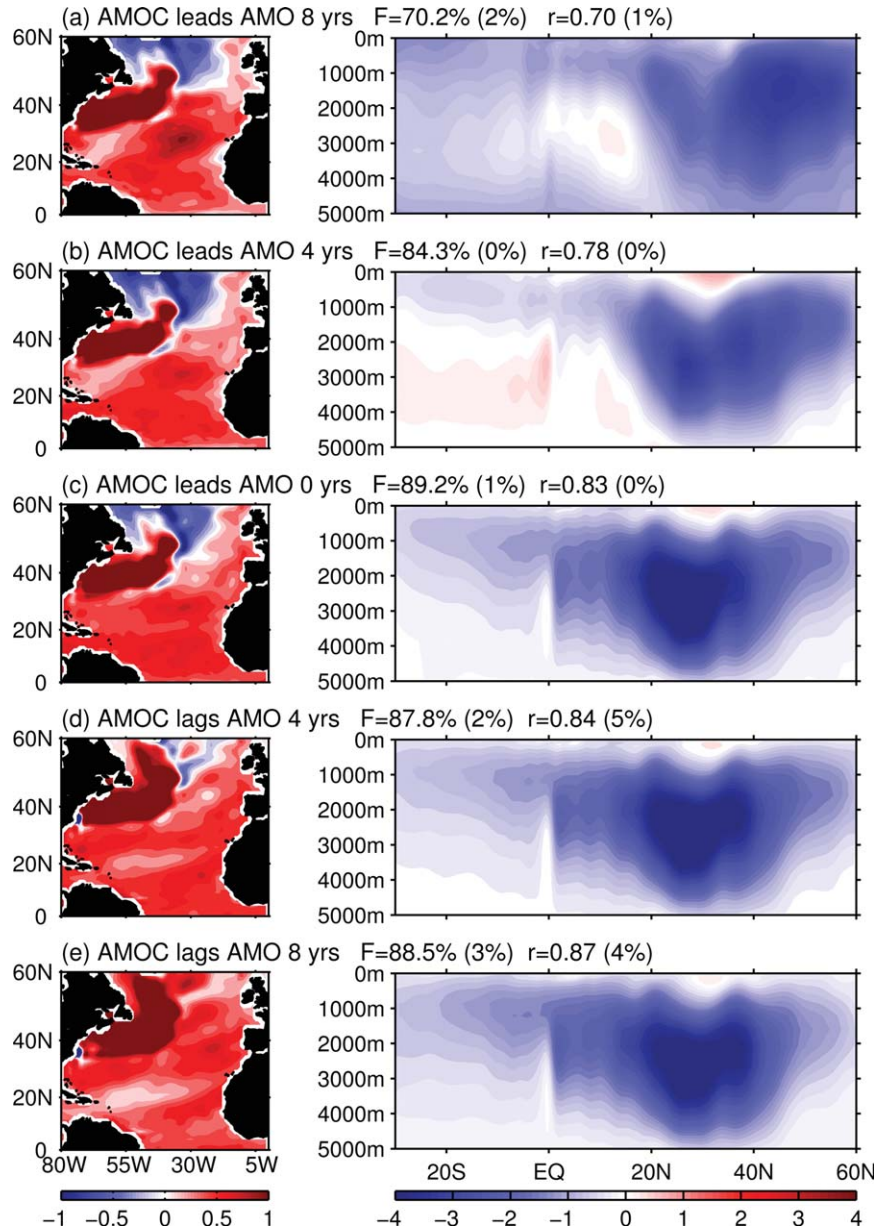


Figure 15. Same as Figure 12 but for the Category II FGOALS-g2 model.

former is easily understood. However, the latter seems to contradict with the traditional notion. This may be due to the influence of salinity on the meridional density gradient. Temperature and salinity usually compensate each other and therefore have complicated influences on the density. The other possible cause is that the AMO spatial pattern is not well reproduced by these coupled models with the largest amplitude occurring not in the higher latitude. This will be discussed in details in the following section. Generally speaking, the results from the MCA analyses are quite similar to the simple lead-lag correlation shown in Figures 10 and 11.

5. Discussion

[28] Observational studies have identified a North Atlantic SST variation on multidecadal timescales [e.g.,

Delworth and Mann, 2000; Wang and Zhang, 2013], which is referred to as the AMO. The warm phases of the AMO occurred during 1860–1880, 1925–1965, and 1995 to the present, and the cool phases during 1905–1925 and 1970–1990. The present paper shows that many of the climate models in CMIP5 are able to reasonably simulate amplitudes and to some extent the durations of the AMO fluctuations; however, they are not able to reproduce the timing of the observed warm and cold phases, particularly in the period of 1900–1960. Similar problems have been found in CMIP3 models [*Medhaug and Furevik, 2011*]. The result is consistent with that of *Ting et al. [2009]* and *Knight [2009]* who argued that the AMO signal is intrinsic to the climate system and not primarily forced by the external forcing. On the other hand, it is also found that a large number of models are not able to capture the observed spatial distribution pattern of the AMO. Some models display the largest

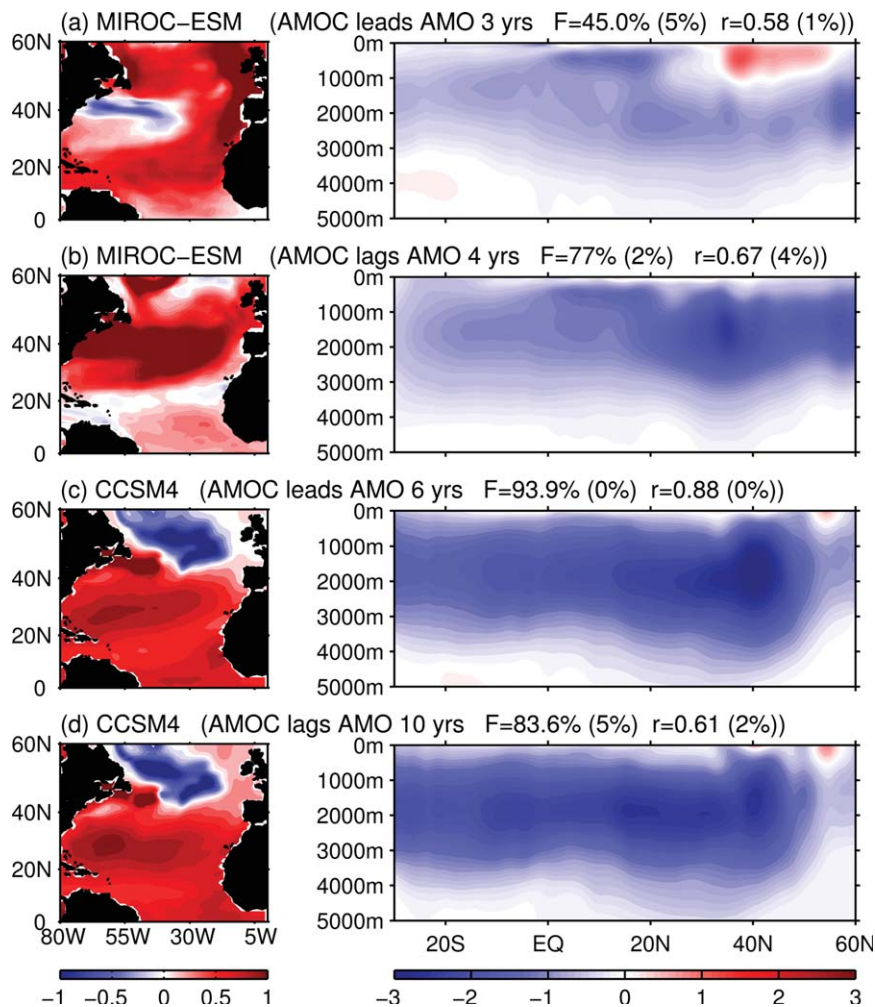


Figure 16. Same as Figure 13 but for the Category II MIROC-ESM and CCSM4 models at selected leads and lags.

amplitude in midlatitudes rather than in the subpolar region as shown in observations.

[29] The AMO and AMOC in CMIP5 models have a similar range of persistence (5–25 years), indicating a potential for decadal predictability. The averaged persistence is a little bit longer than that in CMIP3 [Medhaug and Furevik, 2011]. Spectrum analyses show that the AMOC and AMO have two common energy peaks: One at 20–30 years and the other at 50–70 years. These common features indicate that there could be some relationships between the AMOC and AMO (also see Wang and Zhang [2013]). In 11 out of 18 models, there is a positive (negative) correlation between the AMOC and AMO when the AMOC leads (lags). This indicates that the AMO variability might be a response to the AMOC variations through changes in the northward heat transport. Meanwhile, the AMO can inversely affect the AMOC fluctuations by changing the meridional density gradient. This feature is very similar to the delayed advective oscillator suggested by Lee and Wang [2010]. In these models, the AMOC is the dominant factor to affect the AMO changes and the AMO-induced temperature anomaly can significantly influence the meridional density gradient. Because of these relationships, the

multidecadal oscillation of the AMO and AMOC can be sustained through positive and negative feedbacks.

[30] The passive response of the AMO to the AMOC is illustrated in previous studies based on coupled models [Knight *et al.*, 2005; Delworth *et al.*, 2001]. However, other modeling studies also indicate that the solar variability and/or volcanoes play a role [Hansen *et al.*, 2005; Otterå *et al.*, 2010] or even that the AMO is totally forced by external forcing [Booth *et al.*, 2012]. This may explain why in some models (Category II) a strengthened AMOC does not definitely lead to a warm phase of the AMO. This also implies that even if the AMOC plays an important role in the AMO variability, there are other factors such as externally forced variability or nonpredictive stochastic forcing from the atmosphere that can make a contribution to the AMO.

[31] There are several studies indicating a relationship between the large-scale meridional density gradient and the AMOC [e.g., Thorpe *et al.*, 2001; Wang *et al.*, 2010]. That is, a larger depth integrated density gradient is associated with a stronger AMOC. If more heat and/or freshwater are transported into the North Atlantic deep convection region (Labrador Sea, Irminger Sea, and Nordics Sea), a decreased density in this region will reduce the north-south density

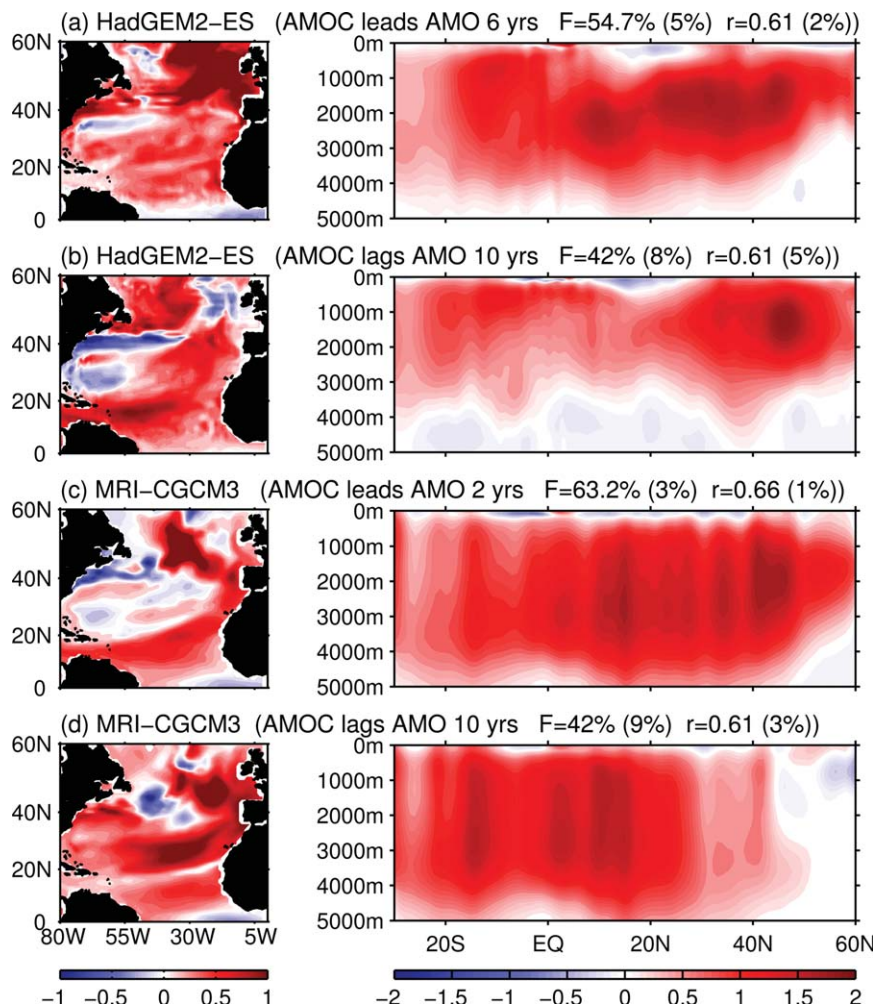


Figure 17. Same as Figure 13 but for the Category III HadGEM2-ES and MRI-CGCM3 models at selected leads and lags.

gradient and thus the upper ocean northward inflow strength. The result will lead to a decreased AMOC. However, the weakened AMOC at the same time will increase the residence time of the water in the subtropical North Atlantic, produce more net evaporation, and lead to a positive salinity anomaly being transported to the sinking region, which in turn restore the meridional density gradient and speed up the AMOC [Otterå *et al.*, 2003]. Because the relative importance of the temperature and salinity anomalies in determining the density in the sinking region varies among models, the influence of the AMO on the AMOC is expected to be highly varied in different models. As shown in Category III models, the AMOC becomes strengthening after a warm AMO phase. This may result from the influence of the salinity. Additionally, the simulated AMO pattern may also explain why the warm phase of the AMO induces the strengthened AMOC. As shown in Figures 17d and 5A, the AMO spatial pattern in MRI-CGCM3 model has its largest warming over the eastern subtropical region, rather than in the subpolar region. This AMO warm phase leads to an increased meridional density gradient and thus a strengthened AMOC.

6. Summary and Conclusion

[32] In this paper, simulated variability of the AMO and the AMOC has been investigated and compared with observations. For the first time, CMIP5 climate models in historical simulations have been used for this purpose. The models show the most energetic variability on multidecadal timescale band both with respect to the AMO and AMOC indices, but with a large intermodel spread in both amplitudes and frequencies. The relationship between the AMOC and AMO in most of the models resembles a delayed advective oscillation proposed for the AMOC [Lee and Wang, 2010]. A strengthening (weakening) of the AMOC is in favor of a warm (cold) phase of the AMO by the anomalous northward (southward) heat transport in the upper ocean, which reversely leads to a slow down (an accelerating) of the AMOC by changes in the meridional density gradient after time of ocean adjustment. This points out that the AMOC and AMO could be interdependent and interactive.

[33] Compared with the observations, a large number of models underestimate the amplitude of the AMO. For the

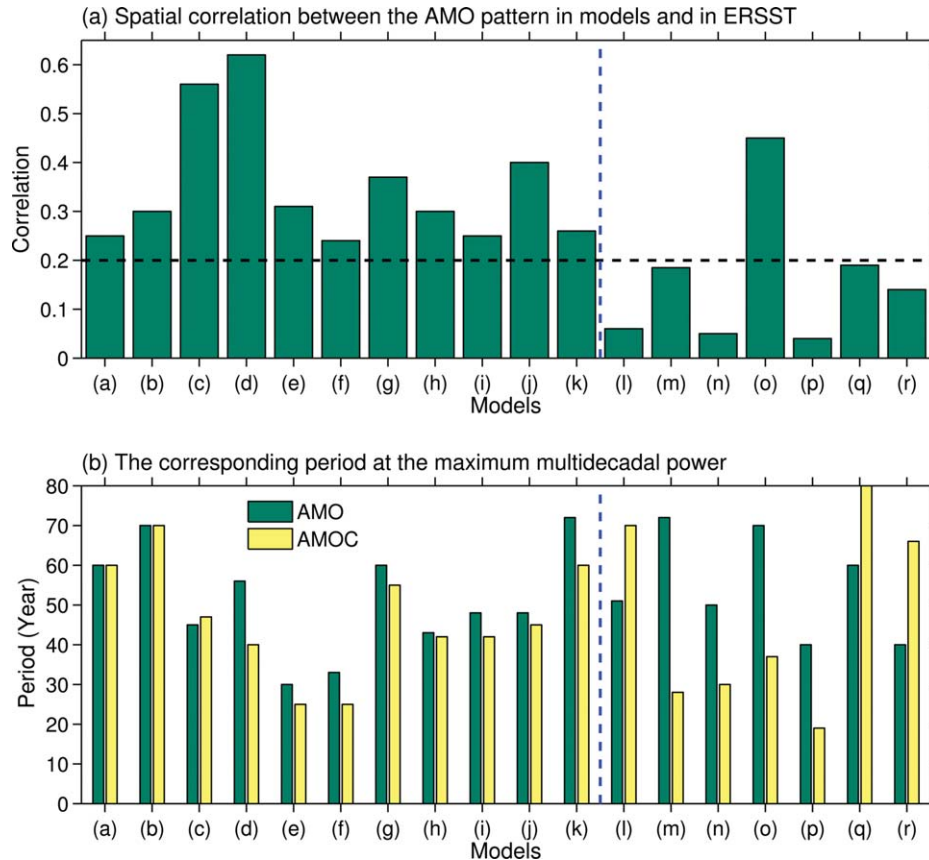


Figure 18. (a) Spatial correlation between the AMO pattern in models and in ERSST and (b) the corresponding periods for the maximum multidecadal AMO power and AMOC power. The x axis denotes different models and their model identifiers are shown in Figure 10.

AMO spatial structure, some of models capture the observed feature, while others cannot reasonably simulate the location of the maximum SST anomaly. CMIP5 models generally show a realistic structure of the overturning circulation, including both the upper Atlantic cell (i.e., the AMOC) and the lower Antarctic overturning cell (AABW), although the AABW in some models penetrates too north and the magnitude is too small. In 16 out of 18 models, the AMOC shows values within the observationally based estimate of the range of 13–24.3 Sv. The relationship between the AMOC and AMO shown in the simple lead-lag correlation can also be obtained by using the MCA method. In 11 out of 18 models, the first MCA mode shows the strengthened (weakened) AMOC is associated with the AMO warm (cold) phase when the AMOC leads, and the warm (cold) AMO phase is accompanied with a slow down (speed up) of the AMOC when the AMO leads. The former can be explained by the AMOC-induced heat transport anomaly and the latter is associated with the AMO-induced anomalous meridional density gradient. In other models, the relationship between the AMOC and AMO becomes more complicated. There are many other factors influencing the AMO and AMOC variability such as external forcing, non-predictable stochastic forcing.

[34] It is interesting to find that the 11 models that are featured by a delayed advective oscillator with a positive (negative) correlation when the AMOC leads (lags) the

AMO share similar frequency of AMO and AMOC and have a good resemblance of AMO spatial pattern to observations. As displayed in Figure 18a, the AMO spatial pattern in 11 models has a larger correlation with the observations than the rest of the models. This indicates that these 11 models have relatively good abilities in capturing the observed AMO spatial pattern. There is an exception for model o (HadGEM2-ES), which simulates the AMO spatial pattern very well. However, it doesn't manifest the relationship between the AMO and AMOC as a delayed advective oscillator. This may arise from the dominant effect of aerosol in the AMO in this specific model [Booth *et al.*, 2012]. Figure 18b shows that the periods for the maximum multidecadal AMO and AMOC power. It can be seen that the significant multidecadal periods for the AMO and AMOC are very similar in these 11 models which have a positive (negative) correlation when the AMOC leads (lags) the AMO. In the rest models, the significant periods for the AMO and AMOC are quite different. This further implies that the delayed advective oscillator mechanism exists in the 11 models.

[35] This study attempts to assess the potential relationship between the AMOC and AMO in CMIP5 historical simulations. However, the length of model simulations is not long enough, so it is very difficult to strictly separate the external variability such as the anthropogenic aerosol from the internal variation. Here we use a simple method

of the linear trend which has been broadly undertaken by many studies, particularly in the observation, to extract the external fluctuations. Although this method may have some artificial effects in the analysis, it still can be considered as a direct and simple method. There is no consensus on how to separate the internal and external variations of the AMO and AMOC. It is unclear if the method described by *Ting et al.* [2009], for example, is definitely better than the simple detrended method. In this paper, we just attempt to give a general assessment of the AMO and AMOC simulations by CMIP5 historical runs. In the future, we will try to use different methods including specific statistical methods and model designs to study the AMO and AMOC.

[36] **Acknowledgments.** We thank three reviewers for their comments and suggestions on the manuscript. This work was supported by grants from National Oceanic and Atmospheric Administration (NOAA) Climate Program Office and the base funding of NOAA Atlantic Oceanographic and Meteorological Laboratory (AOML). The findings and conclusions in this report are those of the author(s) and do not necessarily represent the views of the funding agency.

References

- Booth, B. B. B., N. J. Dunstone, P. R. Halloran, and T. N. Andrews-Bellouin (2012), Aerosols implicated as a prime driver of twentieth-century North Atlantic climate variability, *Nature*, *484*, 228–232.
- Bretherton, C. S., M. Widmann, V. P. Dymnikov, J. M. Wallace, and I. Blade (1999), The effective number of spatial degrees of freedom of a time-varying field, *J. Clim.*, *12*, 1990–2009.
- Bryden, H. L., H. R. Longworth, and S. A. Cunningham (2005), Slowing of the Atlantic meridional overturning circulation at 25°N, *Nature*, *438*, 655–657.
- Cheng, W., and J. C. H. Chiang (2013), Atlantic meridional overturning circulation (AMOC) in CMIP5 models: RCP and historical simulations, *J. Clim.*, *26*, 7187–7197.
- Cunningham, S. A., et al. (2007), Temporal variability for the Atlantic meridional overturning circulation at 26.5°N, *Science*, *317*, 935–937.
- Czaja, A., and C. Frankignoul (2002), Observed impact of North Atlantic SST anomalies on the North Atlantic oscillation, *J. Clim.*, *15*, 606–623.
- Delworth, T. L., and M. E. Mann (2000), Observed and simulated multidecadal variability in the Northern hemisphere, *Clim. Dyn.*, *16*, 661–676.
- Delworth, T. L., S. Manabe, and R. J. Stouffer (1993), Interdecadal variation in the thermohaline circulation in a coupled ocean-atmosphere model, *J. Clim.*, *6*, 1993–2011.
- Deshayes, J., and C. Frankignoul (2008), Simulated variability of the circulation of the North Atlantic from 1953 to 2003, *J. Clim.*, *21*, 4919–4933.
- Dickson, R., J. Lazier, J. Meincke, P. Rhines, and J. Swift (1996), Long term coordinated changes in the convective activity of the North Atlantic, *Prog. Oceanogr.*, *38*, 241–295.
- Eden, C., and J. Willebrand (2001), Mechanisms of interannual to decadal variability of the North Atlantic circulation, *J. Clim.*, *14*, 2266–2280.
- Enfield, D. B., A. M. Mestas-Núñez, and P. J. Trimble (2001), The Atlantic multidecadal oscillation and its relation to rainfall and river flows in the continental US, *Geophys. Res. Lett.*, *28*, 2077–2080.
- Folland, C. K., D. E. Parker, and F. E. Kates (1984), Worldwide marine temperature fluctuations 1856–1981, *Nature*, *310*, 670–673.
- Folland, C. K., D. E. Parker, and T. N. Palmer (1986), Sahel rainfall and worldwide sea temperatures, 1901–85, *Nature*, *320*, 602–607.
- Folland, C. K., A. W. Colman, D. P. Rowell, and M. K. Davey (2001), Predictability of northeast Brazil rainfall and real-time forecast skill, 1987–98, *J. Clim.*, *14*, 1937–1958.
- Folland, C. K., J. Knight, H. W. Linderholm, D. Fereday, S. Ineson, and J. W. Hurrell (2009), The summer North Atlantic oscillation: Past, present, and future, *J. Clim.*, *22*, 1082–1103.
- Frankcombe, L. M., H. A. Dijkstra, and A. von der Heydt (2009), Noise-induced multidecadal variability in the North Atlantic: Excitation of normal modes, *J. Phys. Oceanogr.*, *39*, 220–233.
- Ganachaud, A. (2003), Large-scale mass transports, water mass formation, and diffusivities estimated from World Ocean Circulation Experiment (WOCE) hydrographic data, *J. Geophys. Res.*, *108*, 3213, doi:10.1029/2002JC001565.
- Ganachaud, A., and C. Wunsch (2000), Improved estimates of global ocean circulation, heat transport and mixing from hydrographic data, *Nature*, *408*, 453–457.
- Gastineau, G., and C. Frankignoul (2012), Cold-season atmospheric response to the natural variability of the Atlantic meridional overturning circulation, *Clim. Dyn.*, *39*, 37–57.
- Gastineau, G., F. D. Andrea, and C. Frankignoul (2013), Atmospheric response to the North Atlantic Ocean variability on seasonal to decadal time scales, *Clim. Dyn.*, *40*, 9–10.
- Goldenberg, S. B., C. W. Landsea, A. M. Mestas-Núñez, and W. M. Gray (2001), The recent increase in Atlantic hurricane activity: Causes and implications, *Science*, *293*, 474–479.
- Gray, W. M., J. D. Sheaffer, and C. W. Landsea (1997), Climate trends associated with multidecadal variability of Atlantic hurricane activity, in *Hurricanes: Climate and Socioeconomic Impacts*, edited by H. F. Diaz and R. S. Pulwarty, pp. 15–53, Springer, New York.
- Häkkinen, S. (1999), Variability of the simulated meridional heat transport in the North Atlantic for the period 1951–1993, *J. Geophys. Res.*, *104*, 10,991–11,007.
- Hansen, J., et al. (2005), Earth's energy imbalance: Confirmation and implications, *Science*, *308*, 1431–1435, doi:10.1126/science.1110252.
- Jackson, L., and M. Vellinga (2012), Multidecadal to centennial variability of the AMOC: HadCM3 and a perturbed physics ensemble, *J. Clim.*, *26*, 2390–2407.
- Johnson, G. C. (2008), Quantifying Antarctic bottom water and North Atlantic deep water volumes, *J. Geophys. Res.*, *113*, C05027, doi:10.1029/2007JC004477.
- Knight, J. R. (2009), The Atlantic Multidecadal Oscillation inferred from the forced climate response in coupled general circulation models, *J. Clim.*, *22*, 1610–1625.
- Knight, J. R., R. J. Allan, C. K. Folland, M. Vellinga, and M. E. Mann (2005), A signature of persistent natural thermohaline circulation cycles in observed climate, *Geophys. Res. Lett.*, *32*, L20708, doi:10.1029/2005GL024233.
- Knight, J. R., C. K. Folland, and A. A. Scaife (2006), Climate impacts of the Atlantic Multidecadal Oscillation, *Geophys. Res. Lett.*, *33*, L17706, doi:10.1029/2006GL026242.
- Kravtsov, S., and C. Spanagale (2008), Multidecadal climate variability in observed and modeled surface temperatures, *J. Clim.*, *21*, 1104–1121.
- Lee, S. K., and C. Wang (2010), Delayed advective oscillation of the Atlantic thermohaline circulation, *J. Clim.*, *23*, 1254–1261.
- Lumpkin, R., and K. Speer (2003), Large-scale vertical and horizontal circulation in the North Atlantic Ocean, *J. Phys. Oceanogr.*, *33*, 1902–1920.
- Mann, M. E., and J. M. Lees (1996), Robust estimation of background noise and signal detection in climatic time series, *Clim. Change*, *33*, 409–445.
- McCabe, G. J., M. A. Palecki, and J. L. Betancourt (2004), Pacific and Atlantic Ocean influences on multidecadal drought frequency in the United States, *Proc. Natl. Acad. Sci. U. S. A.*, *101*, 4136–4141.
- Medhaug, I., and T. Furevik (2011), North Atlantic 20th century multidecadal variability in coupled climate models: Sea surface temperature and ocean overturning circulation, *Ocean Sci.*, *7*, 389–404.
- Medhaug, I., H. R. Langehaug, T. Eldevik, T. Furevik, and M. Bentsen (2012), Mechanisms for decadal scale variability in a simulated Atlantic meridional overturning circulation, *Clim. Dyn.*, *39*, 77–93.
- Mestas-Núñez, A. M., and D. B. Enfield (1999), Rotated global modes of non-ENSO sea surface temperature variability, *J. Clim.*, *12*, 2734–2746.
- Msadek, R., and C. Frankignoul (2009), Atlantic multidecadal oceanic variability and its influence on the atmosphere in a climate model, *Clim. Dyn.*, *33*, 45–62.
- Otterå, O. H., H. Drange, M. Bentsen, N. G. Kvamstø, and D. Jiang (2003), The sensitivity of the present-day Atlantic meridional overturning circulation to freshwater forcing, *Geophys. Res. Lett.*, *30*, 1898, doi:10.1029/2003GL017578.
- Otterå, O. H., M. Bentsen, H. Drange, and L. Suo (2010), External forcing as a metronome for Atlantic multidecadal variability, *Nat. Geosci.*, *3*, 688–694.
- Parker, D., C. Folland, A. Scaife, J. Knight, A. Colman, P. Baines, and B. Dong (2007), Decadal to multidecadal variability and the climate change background, *J. Geophys. Res.*, *112*, D18115, doi:10.1029/2007JD008411.
- Rodwell, M. J., and C. K. Folland (2003), Atlantic air-sea interaction and model validation, *Ann. Geophys.*, *46*, 47–56.
- Rowell, D. P. (2003), The impact of Mediterranean SSTs on the Sahelian rainfall season, *J. Clim.*, *16*, 849–862.

- Rowell, D. P., C. K. Folland, K. Maskell, and M. N. Ward (1995), Variability of summer rainfall over tropical North-Africa (1906–92) observations and modelling, *Q. J. R. Meteorol. Soc.*, *121*, 669–704.
- Schott, F. A., J. P. McCreary, and G. C. Johnson (2004), Shallow overturning circulation of the tropical-subtropical oceans, in *Earth Climate: The Ocean-Atmosphere Interaction*, edited by C. Wang, S. Xie, and J. A. Carton, AGU Geophys. Monogr. Series, *147*, 261–304.
- Smethie, W. M., and R. A. Fine (2001), Rates of North Atlantic deep water formation calculated from chlorofluorocarbon inventories, *Deep Sea Res., Part I*, *48*, 189–215.
- Smith, T. M., R. W. Reynolds, T. C. Peterson, and J. Lawrimore (2008) Improvements to 598 NOAA's historical merged land-ocean surface temperature analysis (1880–2006), *J. Clim.*, *21*, 2283–2296.
- Sutton, R. T., and B. Dong (2012), Atlantic Ocean influence on a shift in European climate in the 1990s, *Nat. Geosci.*, *5*, 788–792.
- Sutton, R. T., and D. L. R. Hodson (2005), Atlantic Ocean forcing of North American and European summer climate, *Science*, *309*, 115–118.
- Talley, L. D., J. L. Reid, and P. E. Robbins (2003), Data-based meridional overturning streamfunctions for the global ocean, *J. Clim.*, *16*, 3213–3226.
- Taylor, K. E., R. J. Stouffer, and G. A. Meehl (2012), An overview of CMIP5 and the experiment design, *Bull. Am. Meteorol. Soc.*, *93*, 485–498.
- Thorpe, R. B., J. M. Gregory, T. C. Johns, R. A. Wood, and J. F. B. Mitchell (2001), Mechanisms determining the Atlantic thermohaline circulation response to greenhouse gas forcing in a non flux-adjusted coupled climate model, *J. Clim.*, *14*, 3102–3116.
- Ting, M., Y. Kushnir, R. Seager, and C. Li (2009), Forced and internal twentieth-century SST trends in the North Atlantic, *J. Clim.*, *22*, 1469–1481.
- Ting, M., Y. Kushnir, R. Seager, and C. Li (2011), Robust features of Atlantic multi-decadal variability and its climate impacts, *Geophys. Res. Lett.*, *38*, L17705, doi:10.1029/2011GL048712.
- Trenberth, K. E., and D. J. Shea (2006), Atlantic hurricanes and natural variability in 2005, *Geophys. Res. Lett.*, *33*, L12704, doi:10.1029/2006GL026894.
- Vellinga, M., and P. Wu (2004), Low-latitude freshwater influence on centennial variability of the Atlantic thermohaline circulation, *J. Clim.*, *17*, 4498–4511.
- Wang, C., and S. K. Lee (2009), Co-variability of tropical cyclones in the North Atlantic and the Eastern North Pacific, *Geophys. Res. Lett.*, *36*, L24702, doi:10.1029/2009GL041469.
- Wang, C., and L. Zhang (2013), Multidecadal ocean temperature and salinity variability in the tropical North Atlantic: Linking with the AMO, AMOC and subtropical cell, *J. Clim.*, *26*, 6137–6162.
- Wang, C., S. Dong, and E. Munoz (2010), Seawater density variations in the North Atlantic and the Atlantic meridional overturning circulation, *Clim. Dyn.*, *34*, 953–968.
- Wang, C., S. Dong, A. T. Evan, G. R. Foltz, and S. K. Lee (2012), Multidecadal covariability of North Atlantic sea surface temperature, African dust, Sahel rainfall and Atlantic hurricanes, *J. Clim.*, *25*, 5404–5415.
- Wang, C., L. Zhang, and S.-K. Lee (2013), Response of freshwater flux and sea surface salinity to variability of the Atlantic warm pool, *J. Clim.*, *26*, 1249–1267, doi:10.1175/JCLI-D-12-00284.1.
- Wunsch, C., and P. Heimbach (2006), Estimated decadal changes in the North Atlantic meridional overturning circulation and heat flux 1993–2004, *J. Phys. Oceanogr.*, *36*, 2012–2024.
- Zhang, R. (2008), Coherent surface-subsurface fingerprint of the Atlantic meridional overturning circulation, *Geophys. Res. Lett.*, *35*, L20705, doi:10.1029/2008GL035463.
- Zhang, R. (2010), Latitudinal dependence of Atlantic Meridional Overturning Circulation (AMOC) variations, *Geophys. Res. Lett.*, *37*, L16703, doi:10.1029/2010GL044474.
- Zhang, L., and C. Wang (2012), Remote influences on freshwater flux variability in the Atlantic warm pool region, *Geophys. Res. Lett.*, *39*, L19714, doi:10.1029/2012GL053530.
- Zhang, L., C. Wang, and L. Wu (2012), Low-frequency modulation of the Atlantic warm pool by the Atlantic multidecadal oscillation, *Clim. Dyn.*, *39*, 1661–1671.
- Zhang, L., L. Wu., X. Lin., and D. Wu (2010), Modes and mechanisms of sea surface temperature low-frequency variations over the coastal China seas, *J. Geophys. Res.*, *115*, C08031, doi:10.1029/2009JC006025.
- Zhang, R., et al. (2013), Have aerosols caused the observed Atlantic multidecadal variability?, *J. Atmos. Sci.*, *70*(4), 1135–1144, doi:10.1175/JAS-D-12-0331.1.